Germany), Lys-C was from Wako (Osaka, Japan) and *n*-octyl glucoside was obtained from Dojin (Kumamoto, Japan). MALDI-TOF/MS spectra were obtained using a Voyager linear DE or oMALDI-QSTAR pulsar I instrument (Applied Biosystems, Foster City, CA) operated in delayed-extraction mode. The spectra were calibrated using internal standards, angiotensin III and oxidized insulin B chain.

Electron microscopy

Amphiphysin I, liposomes, dynamin I or truncation constructs of amphiphysin I were mixed under the same conditions described in Methods for '*In vitro* proteolysis of amphiphysin I'. For negative staining, samples were treated as described previously (Yoshida *et al*, 2004) and then observed with a Hitachi H-7100 transmission electron microscope (Tokyo, Japan) at the Central Research Laboratory at Okayama University Medical School.

Transferrin uptake assays

Cos-7 cells were preincubated for 30–60 min in serum-free DMEM (Invitrogen, Carlsbad, CA) at 37°C and then incubated in 25 μg/ml of Alexa Fluor® 546-conjugated transferrin (Invitrogen) for 30 min. The cells were washed in PBS (without Ca^{2+} and Mg^{2+}) buffer and then transferrin uptake was monitored under a confocal laser microscope (FluoView FV300, Olympus, Tokyo, Japan). To quantify the results, signals were estimated in 21–33 randomly chosen fields each with 15–20 cells with EGFP overexpression from five separate experiments.

Hippocampal neuron culture and FM 4–64 labeling

Hippocampal neuron culture was performed as described previously (Tomizawa *et al*, 2003). For transfection of amphiphysin I cDNAs, FL and truncated forms of amphiphysin I cDNAs were subcloned into IRES2-EGFP vector (BD Biosciences). Neuronal transfection of various plasmids including WT amphiphysin I, IRES2-EGFP vector and a truncated form of amphiphysin I (1–392) was carried out using the Nucleofector® system (Amaxa Biosystems, Gaithersburg, MD) according to the manufacturer's instructions.

FM-dye imaging was performed as described previously (Tomizawa *et al*, 2003). Briefly, to load FM 4–64 dye into synaptic vesicles, field stimulation at 20 Hz, 30 s, duration 1.0 ms and intensity 20 V was delivered to the culture through a parallel platinum–iridium electrode immersed into the perfusion chamber. FM 4–64 dye (10 μM, Invitrogen) was present in the perfusion solution from 40 s before stimulation to 40 s after stimulation. After FM 4–64 loading, the culture was rinsed with dye-free perfusion solution for 10 min and fluorescence imaging was performed. An unloading stimulation (10 Hz, 1 min) was delivered to the culture in the dye-free solution to unload the previously loaded dye.

Optical imaging experiments were performed with a Zeiss Axiovert 200 inverted microscope equipped with a CCD camera (Hamamatsu Photonics, Hamamatsu, Japan). Fluorescence images were acquired and analyzed with AquaCosmos software and processed with Photoshop CS and NIH image J software. Images obtained after unloading were used for background subtraction. The intensity of FM 4–64 fluorescence was quantified by measuring the integral FM 4–64 fluorescence intensity of active boutons on subtracted images (loading minus unloading). To compare the results, FM 4–64 fluorescence signals were estimated in 47–55 boutons with EGFP overexpression from five separate experiments.

Animal experiments

Male FVB/NJ mice (25.0–30.0 g, 9 weeks old) were housed individually on a 12-h light/dark schedule with free access to food and water. KA (TOCRIS, Ellisville, MO) and *N*-acetyl-Leu-Leu-methional (ALLM; Merck) were administered by intraperitoneal injection. For preconditioning, the mice were injected with 20 mg/kg KA 3 h before 30 mg/kg KA injection. ALLM (20 mg/kg) was injected 1 h before the preconditioning and once more simultaneously at preconditioning. Mice were continuously monitored and seizures were scored for 3 h according to a previously defined seizure rating scale (Racine, 1972): stage 0, normal; stage 1, immobility; stage 2, forelimb and/or tail extension, rigid posture; stage 3, repetitive movements, head bobbing; stage 4, rearing and falling; stage 5, continuous rearing and falling; stage 6, severe tonic–clonic seizures (jumping). For Western blotting of calpain-dependent amphiphysin I cleavages, hippocampi were obtained from KA-injected mice at each time.

Statistical analysis

Values are reported as the mean ± s.e.m. Data were analyzed using Student's *t*-test to compare two conditions and one-way ANOVA or the Kruskal–Wallis test to compare multiple conditions; $P<0.05$ was considered to be significant.

Supplementary data

Supplementary data are available at *The EMBO Journal* Online (http://www.embojournal.org).

Acknowledgements

We thank P De Camilli for providing amphiphysin I antibodies. This work was supported by the Research Program on Development of Innovative Technology from the Japan Science and Technology Agency (JST), by a grant from the New Energy and Industrial Technology Development Organization (NEDO) and by a Grant-in-Aid for Scientific Research on Priority Areas 'Membrane Traffic' from the Ministry of Education, Science, Sports and Culture of Japan.

Competing interests statement

The authors declare that they have no competing financial interests.

References

Ben-Ari Y (1985) Limbic seizure and brain damage produced by kainic acid: mechanism and relevance to human temporal lobe epilepsy. *Neuroscience* **14:** 375–403

Costantin L, Bozzi Y, Richichi C, Viegi A, Antonucci F, Funicello M, Gobbi M, Mennini T, Rossetto O, Montecucco C, Maffei L, Vezzani A, Caleo M (2005) Antiepileptic effects of botulinum neurotoxin E. *J Neurosci* **25:** 1943–1951

Cousin MA, Robinson PJ (2001) The dephosphins: dephosphorylation by calcineurin triggers synaptic vesicle endocytosis. *Trends Neurosci* **24:** 659–665

Czogalla A, Sikorski AF (2005) Spectrin and calpain: a 'target' and a 'sniper' in the pathology of neuronal cells. *Cell Mol Life Sci* **62:** 1913–1924

Evergren E, Marcucci M, Tomilin N, Low P, Slepnev V, Andersson F, Gad H, Brodin L, De Camilli P, Shupliakov O (2004) Amphiphysin is a component of clathrin coats formed during synaptic vesicle recycling at the lamprey giant synapse. *Traffic* **5:** 514–528

Granseth B, Odermatt B, Royle SJ, Lagnado L (2006) Clathrin-mediated endocytosis is the dominant mechanism of vesicle retrieval at hippocampal synapses. *Neuron* **51:** 773–786

Lee MS, Kwon YT, Li M, Peng J, Friedlander RM, Tsai LH (2000) Neurotoxicity induces cleavage of p35 to p25 by calpain. *Nature* **405:** 360–364

Liang S, Wei FY, Wu YM, Tanabe K, Abe T, Oda Y, Yoshida Y, Yamada H, Matsui H, Tomizawa K, Takei K (2007) Major Cdk5-dependent phosphorylation sites of amphiphysin 1 are implicated in the regulation of the membrane binding and endocytosis. *J Neurochem*, in press

Liu JP, Powell KA, Sudhof TC, Robinson PJ (1994) Dynamin I is a Ca^{2+}-sensitive phospholipid-binding protein with very high affinity for protein kinase C. *J Biol Chem* **269:** 21043–21050

Lothman EW, Collins RC (1981) Kainic acid induced limbic seizures: metabolic, behavioral, electroencephalographic and neuropathological correlates. *Brain Res* **218:** 299–318

Okada M, Zhu G, Yoshida S, Kanai K, Hirose S, Kaneko S (2002) Exocytosis mechanism as a new targeting site for mechanisms of action of antiepileptic drugs. *Life Sci* **72:** 465–473

Peter BJ, Kent HM, Mills IG, Vallis Y, Butler PJ, Evans PR, McMahon HT (2004) BAR domains as sensors of membrane curvature: the amphiphysin BAR structure. *Science* **303:** 495–499

Posmantur RM, Kampfl A, Liu SJ, Heck K, Taft WC, Clifton GL, Hayes RL (1996) Cytoskeletal derangements of cortical neuronal processes three hours after traumatic brain injury in rats: an immunofluorescence study. *J Neuropathol Exp Neurol* **55:** 68–80

Racine RJ (1972) Modification of seizure activity by electrical stimulation. II. Motor seizure. *Electroencephalogr Clin Neurophysiol* **32:** 281–294

Rami A (2003) Ischemic neuronal death in the rat hippocampus: the calpain–calpastatin–caspase hypothesis. *Neurobiol Dis* **13:** 75–88

Saido TC, Yokota M, Nagao S, Yamaura I, Tani E, Tsuchiya T, Suzuki K, Kawashima S (1993) Spatial resolution of fodrin proteolysis in postischemic brain. *J Biol Chem* **268:** 25239–25243

Sara Y, Mozhayeva MG, Liu X, Kavalali ET (2002) Fast vesicle recycling supports neurotransmission during sustained stimulation at hippocampal synapses. *J Neurosci* **22:** 1608–1617

Sessoms JS, Chen SJ, Chetkovich DM, Powell CM, Roberson ED, Sweatt JD, Klann E (1992) Ca^{2+}-induced persistent protein kinase C activation in rat hippocampal homogenates. *Second Messengers Phosphoproteins* **14:** 109–126

Shupliakov O, Low P, Grabs D, Gad H, Chen H, David C, Takei K, De Camili P, Brodin L (1997) Synaptic vesicle endocytosis impaired by disruption of dynamin-SH3 domain interactions. *Science* **276:** 259–263

Slepnev VI, Ochoa GC, Butler MH, Grabs D, De Camilli P (1998) Role of phosphorylation in regulation of the assembly of endocytic coat complexes. *Science* **281:** 821–824

Stevens CF, Wesseling JF (1999) Identification of a novel process limiting the rate of synaptic vesicle cycling at hippocampal synapses. *Neuron* **24:** 1017–1028

Sun JY, Wu XS, Wu LG (2002) Single and multiple vesicle fusion induce different rates of endocytosis at a central synapse. *Nature* **417:** 555–559

Takei K, Slepnev VI, Haucke V, De Camilli P (1999) Functional partnership between amphiphysin and dynamin in clathrin-mediated endocytosis. *Nat Cell Biol* **1:** 33–39

Tan TC, Valova VA, Malladi CS, Graham ME, Berven LA, Jupp OJ, Hansra G, McClure SJ, Sarcevic B, Boadle RA, Larsen MR, Cousin MA, Robinson PJ (2003) Cdk5 is essential for synaptic vesicle endocytosis. *Nat Cell Biol* **5:** 701–710

Tomizawa K, Ohta J, Matsushita M, Moriwaki A, Li ST, Takei K, Matsui H (2002) Cdk5/p35 regulates neurotransmitter release through phosphorylation and downregulation of P/Q-type voltage-dependent calcium channel activity. *J Neurosci* **22:** 2590–2597

Tomizawa KS, Sunada S, Lu YF, Oda Y, Kinuta M, Ohshima T, Saito T, Wei FY, Matsushita M, Li ST, Tsutsui K, Hisanaga S, Mikoshiba K, Takei K, Matsui H (2003) Cophosphorylation of amphiphysin I and dynamin I by Cdk5 regulates clathrin-mediated endocytosis of synaptic vesicles. *J Cell Biol* **163:** 813–824

Wang LY, Kaczmarek LK (1998) High-frequency firing helps replenish the readily releasable pool of synaptic vesicles. *Nature* **394:** 384–388

Wigge P, McMahon HT (1998) The amphiphysin family of proteins and their role in endocytosis at the synapse. *Trends Neurosci* **21:** 339–344

Wu HY, Tomizawa K, Oda Y, Wei FY, Lu YF, Matsushita M, Li ST, Moriwaki A, Matsui H (2004) Critical role of calpain-mediated cleavage of calcineurin in excitotoxic neurodegeneration. *J Biol Chem* **279:** 4929–4940

Wu LG (2004) Kinetic regulation of vesicle endocytosis at synapses. *Trends Neurosci* **27:** 548–554

Wu LG, Betz WJ (1998) Kinetics of synaptic depression and vesicle recycling after tetanic stimulation of frog motor nerve terminals. *Biophys J* **74:** 3003–3009

Yoshida Y, Kinuta M, Abe T, Liang S, Araki K, Cremona O, Di Paolo G, Moriyama Y, Yasuda T, De Camilli P, Takei K (2004) The stimulatory action of amphiphysin on dynamin function is dependent on lipid bilayer curvature. *EMBO J* **23:** 3483–3491

Yoshida Y, Takei K (2005) Stimulation of dynamin GTPase activity by amphiphysin. *Methods Enzymol* **404:** 528–537

Zhang B, Zelhof AC (2002) Amphiphysins: raising the BAR for synaptic vesicle recycling and membrane dynamics. Bin-amphiphysin-Rvsp. *Traffic* **3:** 452–460

Zucker RS (1989) Short-term synaptic plasticity. *Annu Rev Neurosci* **12:** 13–31

GENE DELIVERY

ELSEVIER

Available online at www.sciencedirect.com

ScienceDirect

Journal of Controlled Release 118 (2007) 348–356

journal of controlled release

www.elsevier.com/locate/jconrel

Characterization of bio-nanocapsule as a transfer vector targeting human hepatocyte carcinoma by disulfide linkage modification

Tadahiro Nagaoka [a,1], Takayuki Fukuda [a,1], Shinnosuke Yoshida [a], Hirohito Nishimura [a], Dongwei Yu [a,e], Shun'ichi Kuroda [b], Katsuyuki Tanizawa [b], Akihiko Kondo [c], Masakazu Ueda [d], Hidenori Yamada [a], Hiroko Tada [a], Masaharu Seno [a,f,*]

[a] *Department of Medical Bioengineering, Graduate School of Natural Science and Technology, Okayama University, 3-1-1 Tsushima-Naka Okayama 700-8530, Japan*

[b] *Institute of Scientific and Industrial Research, Osaka University, 8-1 Mihogaoka, Ibaraki, Osaka 567-0047, Japan*

[c] *Faculty of Engineering, Kobe University, 1-1 Rokkodai, Nada, Kobe, Hyogo 657-8501, Japan*

[d] *Keio University, School of Medicine, 35 Shinanomachi, Shinjuku-ku, Tokyo 160-8582, Japan*

[e] *Beacle Inc., Okayama Research Park Incubation Center, 5303 Haga, Okayama 701-1221, Japan*

[f] *Research Center for Biomedical Engineering, Okayama University, 3.1.1 Tsushima-Naka, Okayama 700-8530, Japan*

Received 5 September 2006; accepted 12 December 2006
Available online 28 December 2006

Abstract

The bio-nanocapsules (BNCs) composed of the recombinant envelope L-protein of hepatitis B virus constitute efficient delivery vectors specifically targeting human hepatocytes. Here, we have tried to enhance the stability of the BNCs because the L-proteins in the BNCs were aggregated due to random disulfide bridging when stored for a long period at 4 °C. The envelope protein contains fourteen cysteine residues in the S domain. Aggregation of the envelope proteins might be avoided if unessential cysteine residues are replaced or removed because the irreversible alkylation of the free sulfhydryl group protects against the aggregation and enhances the efficiency of encapsulation. In this study, the possibility of reducing the number of cysteine residues in the S domain to enhance the stability of the BNCs was assessed. The replacement of each cysteine residue by site-directed mutation showed that nine of fourteen cysteine residues were not essential to obtaining BNCs secreted into the culture media. Furthermore, upon evaluating the combination of these mutations, it was found that eight residues of replacement were acceptable. The mutant BNCs with replaced eight cysteine residues were not only more resistant against trypsin, but also more effective in transducing genes into human hepatoma-derived HepG2 cells than the original type BNC. Thus, we demonstrated that the minimized number of cysteine residues in the S domain could enhance the stability of the BNCs.

Keywords: Bio-nanocapsule; HBV surface antigen; Delivery vector; Hepatocyte specific targeting; Enhanced stability

1. Introduction

A molecular targeting method that transfers drugs efficiently and safely in a cell type specific manner has been a subject of great attention in the development of a novel drug delivery system (DDS). In general, recent DDS technologies are based on carriers that are categorized as two independent methods, viral and non-viral. Each has its advantages and disadvantages. Viral DDS systems, which exploit viruses, such as retroviruses, adenovirus, adeno-associated virus and lentivirus, have been developed as gene transfer procedures for efficient transduction. However, the patients

Abbreviations: DDS, Drug delivery system; BNC, Bio-nanocapsule; DMEM, Dulbecco's modified Eagle medium; HBV, Hepatitis B virus; GFP, Green fluorescent protein; EIA, Enzyme immunoassay; SDS-PAGE, Sodium dodecyl sulfate polyacrylamide gel electrophoresis.

* Corresponding author. Department of Medical Bioengineering, Graduate School of Natural Science and Technology, Okayama University, 3-1-1 Tsushima-Naka Okayama 700-8530, Japan. Tel./fax: +81 86 251 8216.
E-mail address: mseno@cc.okayama-u.ac.jp (M. Seno).

[1] These two authors equally contributed to this paper.

0168-3659/$ - see front matter © 2006 Elsevier B.V. All rights reserved.
doi:10.1016/j.jconrel.2006.12.020

would have to face the risks of not only having the viral genome integrated into their own genomes, but also of having genes transferred to unexpected cells or tissues in a non-specific manner, resulting in serious diseases, such as cancer [1,2]. A non-viral system, represented by cationic liposome or polyethylene glycol, is considered to be rather safer than a viral system. However, liposome as a transfer vector still needs improvement in order to confer as much efficiency as viral vectors, and specificity on the target cells or tissues [3]. The development of novel DDS vectors with the advantages of both vectors is eagerly awaited [4–6].

Over the last decade, recombinant envelope proteins have been developed as vaccines for hepatitis B virus (HBV) [7]. The envelope of HBV is composed mainly of three closely related surface proteins that are known as the large (L), the middle (M) and the small (S) proteins. They are encoded in one open reading frame of HBV genome translated from three different in-frame initiation sites. When these proteins were expressed, each S-, M- and L-protein was found to form hollow virus-like nanoparticles. The particle composed of L-protein showed, in particular, a specific affinity to human hepatocytes due to the hepatocyte recognition site localized in the amino terminus [8–12]. For the purpose of developing safe and efficient DDS vectors having a targeting potential for specific cells or tissues, we exploited the nanoparticles composed of recombinant envelope protein as bionanocapsule (BNC) prepared from mammalian cells or yeast cells. The BNC composed of L-protein (L-BNC) is a sphere that has an average diameter of 80 nm, which has been observed under atomic force microscope of about 110 molecules of L-protein [13]. This nanoparticle formation is also confirmed under thin section electron microscope [14]. We found that the L-BNC was extremely useful as a vector to deliver genes and pharmaceutical drugs to the human liver in vivo cells, as well as in vitro [15].

However, we experienced aggregation of envelope proteins in the BNCs during long-term storage. We report here that the aggregation is due to the false disulfide bridges and that replacement of cysteine residues in the L-protein enhances the stability of the BNCs.

2. Materials and methods

2.1. Cell culture

COS7 cells were maintained at 37 °C under 5% CO_2 in Dulbecco's modified Eagle medium (DMEM) supplemented with 5% fetal bovine serum (FBS) and 0.1% sodium bicarbonate. HepG2 cells and WiDr cells were maintained at the same conditions, but with 10% FBS.

2.2. Preparation of the L-BNCs in yeast cells

The L-BNCs were produced in *Saccharomyces cerevisiae* AH22$^-$ transformed with the L-protein expression plasmid pGLDLIIP39-RcT and purified as previously described [16].

2.3. Alkylation of L-BNCs with iodomonoacetic acid (IAA)

During purification of L-BNC, IAA was added to the yeast extracts to modify free SH-groups, thereby preventing them from forming false disulfide bridges. IAA was added to 10 mM 15 min before the precipitation of L-BNC with PEG6000 so that IAA could be removed after reaction.

2.4. Comparison of calcein encapsulation into L-BNC with/without IAA modification

Calcein (Dojindo, Japan) was mixed at 1 mM with 240 μg of L-BNCs with or without IAA modification in 500 μl of PBS. This was followed by electroporation with a Gene Pulser II electroporation system (Bio-Rad, VA) in a 4-mm cuvette, at 50 V and 750 μF. After removal of free calcein by gel filtration, calcein incorporated into BNCs was measured by a fluorescence image analyzer LAS-1000 (Fujifilm, Japan).

2.5. Expression of the mutant L-BNCs

The DNA fragment coding of the HBV L-protein that was fused to the secretion signal of chicken lysozyme was inserted downstream of SR alpha promoter to construct the expression vector pBO441. To replace the cysteine residues with serine or alanine residues, the gene for the L-protein was subjected to site-directed mutagenesis. Each resulting plasmid was introduced into COS7 cells by a Gene Pulser II. After 15 h, the medium was replaced by CHO-SFM II (Invitrogen, CA). Four days after transfection, the conditioned medium was collected and concentrated by a Vivaspin 20 (MWCO 1000 kDa, Vivascience, Germany). The BNCs and the derivatives in the conditioned media were immunologically detected and quantified with the Abbott IMx HBsAg assay system (Abbott Laboratories, IL) in the series of two-fold dilution. All the tests were performed and interpreted in accordance with the manufacturer's recommendation. Standard curve of EIA was evaluated with the positive control of HBsAg supplied with the system and antigen in the range of 10–100 ng/ml was estimated. Each sample was measured in triplicates and standard deviation was calculated.

3. Detection of the L-protein and its derivatives by Western blotting

The BNCs in the conditioned media were immunoprecipitated with anti-S antibody conjugated to microparticles, a component of the Abbott IMx HBsAg assay system, and then subjected to SDS-PAGE and Western blotting. The blots were probed with anti-S goat IgG conjugated to biotin and anti-biotin rabbit IgG conjugated to alkaline phosphatase. Immunoreactive bands were detected with the Phototope-Star Chemiluminescent Detection Kit (New England Biolabs, MA). The bands detected were densitometorically analyzed using NIH Image.

3.1. Protease protection assay

The BNCs were immunoprecipitated by anti-S antibody, and treated with various concentration of trypsin for an hour at 37 °C. The digestion fragments were detected using Western blotting, as described above.

3.2. Evaluation of the effects of reducing reagent, and oxidation on the L-BNCs

L-BNCs were treated with various concentration of reducing reagent dithiothreitol (DTT) for 10 min at 25 °C. The L-proteins were analyzed by SDS-PAGE and silver staining. L-BNCs were oxidized, on the other hand, by vigorous agitation at 25 °C. The L-proteins were then analyzed by SDS-PAGE in the presence of 1 mM DTT. Density of the protein bands were measured by Image J<http://rsb.info.nih.gov/ij/> and the time course changes of density were plotted.

3.3. Transduction of DNA into HepG2 cells with BNCs

Prior to transfection, HepG2 cells were seeded into the 8-well chamber slide (Nalge-Nunc international). On the following day, green fluorescent protein (GFP) expression plasmid pEGFP-N1 (Clontech Labs., CA) was introduced into the BNCs by electroporation at 50 V and 750 μF and added into the culture media of HepG2 cells. The final culture volume was adjusted to 500 μl/well. Three days after transfection, the transduction of the plasmid DNA was evaluated by the GFP fluorescence in HepG2 cells under confocal laser scanning microscopy (Carl Zeiss, Germany). The infectious efficiency was evaluated by mean of green color intensity of confocal microscopic images using RGB histogram in Image J.

4. Results

4.1. Stability of L-BNC

Our L-BNCs are efficient transfer vectors with which to target human hepatocytes. However, the L-proteins, the major component of an L-BNC, were difficult to observe, when analyzed on SDS-PAGE without DTT following the long-term storage of the L-BNCs at 4 °C (Fig. 1A lane 1 and Fig. 1B lane 3). In this experiment, we compared freshly prepared L-BNC and purified L-BNCs, which had been stored at 4 °C in PBS for periods of two, four, and nine months. When the L-BNCs were treated with 10 mM DTT for 5 min at 98 °C prior to the electrophoresis, all preparations showed bands at a molecular mass of 47 kDa (Fig. 1A, lanes 8 to 10). However, the lower concentrations of DTT, such as 0.5 or 1 mM, were ineffective on the L-BNCs that were kept for a long term (Fig. 1A, lanes 2 to 7). The longer the storage period became, the tighter appeared to be the interaction of L-protein via disulfide bridges.

To prevent cysteine residues in L-protein from false or random disulfide bonds, we modified the free sulfhydryl group of L-protein with IAA at the first step of preparation from the cell extracts. The SDS-PAGE assessment with DTT described above implies freshly prepared BNC should be free from unessential disulfide bridges. IAA reaction in this stage will not allow further formation of disulfide bridges in L-proteins. They should be kept as many as those just produced in the cells even after the whole purification procedures. When the BNCs modified with IAA were analyzed by SDS-PAGE without DTT, L-protein was shown as monomeric and dimeric forms,

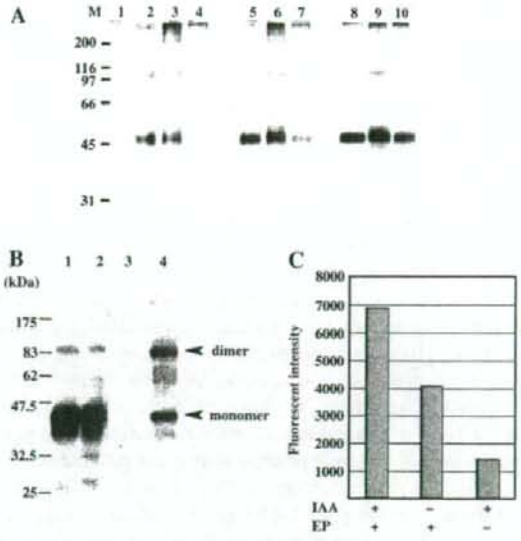

Fig. 1. The sensitivity of L-BNCs to reducing reagent. (A) The L-BNCs from yeast were kept at 4 °C in the refrigerator for two months (lanes 1, 2, 5 and 8), four months (lanes 3, 6 and 9) and nine months (4, 7 and 10). Prior to electrophoresis, these BNCs were treated with 0.5 mM DTT followed by incubation at 25 °C for 10 min (lanes 2, 3 and 4), 1 mM DTT followed by incubation at 25 °C for 10 min (lanes 5, 6 and 7), or 10 mM DTT followed by incubation at 100 °C for 10 min (lanes 8, 9 and 10). These L-BNCs were electrophoresed with or without DTT treatment (lane 1) and the presence of each protein was detected by silver staining. The monomeric form of L-protein was shown as the main band at about 47 kDa, and multimeric form of L-protein appeared at a higher molecular weight or at the top of the gel. (B) The wild type L-BNC (lanes 1 and 3) and the L-BNC modified with IAA (lanes 2 and 4) were analyzed by Western blotting in the presence of, or absence of, 10 mM DTT (lanes 1 and 2, and lanes 3 and 4 respectively). (C) The calcein was encapsulated into the L-BNC and the L-BNC modified with IAA by electroporation. The residual calcein was removed by gel filtration and the fluorescence from the fraction containing 240 μg of L-BNC was measured by LAS-1000.

while intact L-protein in BNCs was not (Fig. 1B). Furthermore, it was observed that the loading of calcein into the BNCs by electroprotation was more efficient when using BNC modified with IAA, rather than with the unmodified BNC (Fig. 1C).

4.2. Essential cys residues for secretion of L-BNC

Consequently, we hypothesized that dispensable inter-/intra-molecular S–S cross-linking would occur in L-protein randomly, with the result that the stability and ability to function as a carrier of BNCs would be destroyed. The unwanted S–S bridges made the formation of the BNCs so tight that the loading efficiency of substances was reduced. It should be important to keep the L-BNC flexible in order to maintain the optimal L-BNC encapsulation efficiency. Hence, we thought that as many as possible unessential cysteine residues should be replaced. Each cysteine residue in the hydrophobic region was replaced with alanine, whereas others in the hydrophilic region were replaced with serine (Fig. 2 and Table 1). The mutant plasmids were transiently expressed in COS7 cells and the amount of the mutant BNCs secreted into the media were

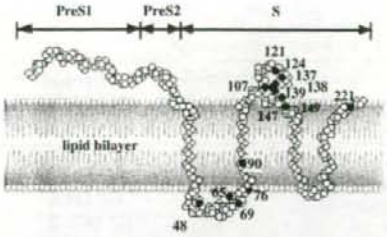

Fig. 2. Speculative secondary-structure model for HBsAg L-protein in the membrane. The L-protein consists of Pre-S1 and Pre-S2 domains followed by S domain. Pre-S1 contains the sequence for the specific binding to human hepatocytes. Pre-S2 is responsible for the association with the polymerized albumin-mediated interaction and for the integration into the membrane. S domain is indispensable for an L-protein to be spun in the lipid bilayer membrane (gray line). The cysteine residues in the S domain are depicted as black circles with the numbers of their positions in the S domain. Then cysteines' residue located in the hydrophobic region, 76, 90, 107, 147, 149 and 221, was replaced with alanine and that of the others located in the hydrophilic region, 48, 65, 69, 121, 124, 137, 138 and 139, was replaced with serine by site-directed mutation.

quantified by EIA system and qualified by immunoprecipitation and Western blotting. This assay system, IMx HBsAg, is based on highly sensitive sandwich EIA aiming at the same epitope localized in the surface region of S domain in L-protein so that it is important for one antigen to have multiple epitopes to be detected. Namely, this one antigen should be a form of virus like particle, which is soluble in aqueous phase. In this case the virus like particle is L-BNC. Since L-protein is a typical transmembrane type protein (Fig. 2), random aggregation of this protein would make insoluble precipitates in denatured state, which could not be detected in EIA. Taking this into consideration, we considered the mutant L-proteins prepared in this study as nanocapsules if they are detected by EIA in aqueous phase.

Each secreted amount of BNC with a single mutation was represented by the percentage relative to that of wild type BNC in Table 1. Each mutation of the cysteine residues at 76, 139, 147, 149 and 221 facilitated the secretion of the BNC remarkably without affecting the essential disulfide bonds, and the mutation of cysteine residue at 90 did not change the level of secretion. Still, more than 50% of the secreted wild type of BNC was detected in the mutations of cysteine residues at 107, 137 and 138. The mutation of cysteine residues at 48, 65, 69, 121 and 124 did not show detectable secretions of BNC. From the results, cysteine residues at 76, 90, 147, 149 and 221 were found dispensable for the secretion. On the other hand, cysteine residues at 48, 65, 69, 121 and 124 were found to be essential for the secretion of BNCs.

Western blot analysis exhibited the characteristic patterns of wild type and derivative mutant L-proteins (Fig. 3). A number of immunoreactive bands were detected in wild type BNCs due to *N*-glycosylation in PreS1, PreS2 and S domain, and also due to alternative translations for M- and S-proteins. The five main bands in wild type L-BNC are recognized to be: (1) the 44 kDa glycosylated form (gpL 44) (2) the 47 kDa glycosylated form (gpL 47) of L-protein (3) the 36 kDa glycosylated form of M-protein (gpM 36) (4) the 28 kDa glycosylated form of S-protein (gpS 28) and (5) the nonglycosylated forms of M and S, which were undetectable. (Fig. 3, lane 1 and 9) [17]. All proteins with mutations at each single cysteine residue displayed characteristic patterns different from that of wild type. In the mutation of cysteine residues at 48, 65 and 69, the bands of L-protein from secreted BNCs were hardly detected (Fig. 3, lanes 2 to 4), and a small number of bands were detected in the mutation of cysteine residues at 121, 124 and 139 (Fig. 3, lanes 8, 10, 13). As for the other mutations of cysteine residues at 76, 90, 107, 137, 138, 147, 149 and 221, the bands of gpL44 and gpL47 were detected almost at the same level as those in the wild type. The results of the Western blot analysis are almost consistent with those of EIA analysis, except for mutations of cysteine residues at 107 and 139.

The results of EIA should indicate that BNC has been detected, rather than the Western blotting, which detects denatured proteins on the membrane filter. For this reason, we concluded that cysteine residue 139 was dispensable, but have withheld any conclusion about cysteine residue at 107. As a consequence, the experiments demonstrated completely that cysteine residues at 76, 90, 137, 138, 139, 147, 149 and 221 were dispensable for the assembly and secretion of the BNCs.

In order to design the most suitable BNCs for the transfer vector, we further assessed the combinations of these nine mutations. As summarized in Table 2, various combinations of the mutation were investigated for the ability to form BNCs. The amounts of the secreted BNCs were estimated by EIA and shown as the percentage relative to that of wild type BNC. In these multiple mutation experiments, cysteine residues at 48, 65, 69, 107, 121 and 124 were not included since these mutations had decreased the apparent production of BNC in the single mutation experiment described above. Because the cysteine residue at 90 was considered to be located in the trans-membrane and the mutation of this residue did not change

Table 1
Production of BNCs with single mutation

Positions of cysteine residues replaced[a]	Immunoreactivity as HBsAg (%)[b]
Cys/48/Ser	21.0±3.0
Cys/65/Ser	21.3±9.0
Cys/69/Ser	22.0±8.6
Cys/76/ Ala	241.0±94.0
Cys/90/ Ala	93.5±4.5
Cys/107/ Ala	56.0±8.5
Cys/121/Ser	14.0±8.5
Cys/124/Ser	13.7±8.7
Cys/137/Ser	65.7±10.7
Cys/138/Ser	58.0±31.9
Cys/139/Ser	186.5±46.3
Cys/147/ Ala	236.3±64.5
Cys/149/ Ala	167.0±66.3
Cys/221/ Ala	142.5±39.1

[a] The name of each mutant BNC indicates the position of the cysteine residue that was replaced by the amino acid, Ser or Ala. The amino acid number is its position in the S region.

[b] The amount of wild type L- and mutant BNCs secreted into the culture media of COS7 cells was estimated by enzyme immunoassay. The averages of the EIA values of each BNC were calculated as a percentage of that of the wild type L-BNC. The standard deviation (S.D.) in the right column was obtained from triplicates of independent experiments.

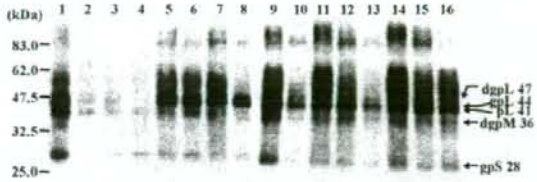

Fig. 3. Analysis of the L-proteins with single substitution at cysteine residues. Wild type (lanes 1 and 9) and mutants (lane 2, C/48/S; lane 3, C/65/S; lane 4, C/69/S; lane 5, C/76/A; lane 6, C/90/A; lane 7, C/107/A; lane 8, C/121/S; lane 10, C/124/S; lane 11, C/137/S; lane 12, C/138/S; lane 13, C/139/S; lane 14, C/147/A; lane 15, C/149/A; lane 16, C/221/A) of BNCs expressed in COS7 cells were immunoprecipitated with anti-S monoclonal antibody conjugated with agarose beads and detected by anti-S polyclonal antibody in Western blotting. SDS polyacrylamide gel electrophoresis was carried out in reducing conditions. The arrows indicate the position of glycosylated (gpS 28) S-protein, diglycosylated (dpM 36) M-protein and glycosylated (gpL 44) and diglycosylated (dpL 47) L-protein. The migration of marker protein (molecular masses in kDa) is shown at the left.

Table 2
Production of BNCs with multiple mutations

Positions of cysteine residues simultaneously replaced[a]	Immunoreactivity as HBsAg (%)[b]
76/90	167.7±30.3
90/139	222.0±71.9
90/147	326.7±71.6
90/149	154.7±86.6
90/221	108.7±25.0
76/90/221	157.0±12.8
76/90/149/221	207.3±62.8
76/90/139/149/221	114.0±22.6
76/90/147/149/221	112.0±40.3
76/90/139/147/149/221	86.3±21.3
76/90/138/139/147/149/221	67.3±7.8
76/90/137/139/147/149/221	97.0±34.4
76/90/137/138/139/147/149/221	80.0±32.3
76/90/107/137/138/139/147/149/221	45.0±18.5

[a] The numbers in the left column represent the position of the cysteine residues, which were substituted as shown in Table 1.
[b] The immunoreactivity of mutant BNCs were measured as described in Table 1.

the productivity of the BNC, this mutation was added to the mutation combination of the cysteine residues at 76, 139, 147, 149 and 221. Each of the latter resulted in greater productivity than that afforded by use of the wild type. All of the double mutants demonstrated more efficient production of BNCs than did the wild type. In fact, the two double mutants, 76/90 and 90/221, gave such good productivity that production of only the triple-mutant 76/90/221 was assessed. As a result, the triple mutant showed an expression level of 157% better than that of wild type. On this basis, we then designed further mutations of quadruple mutations at cysteine residues of 76/90/149/221, which showed a good expression level of 207%. The expression level of quintuple mutations at either cysteine residues at 76/90/139/149/221 or 76/90/147/149/221 was as much as that of the wild type. The sextuple mutations at all of the cysteine residues at 76/90/139/147/149/221 gave an almost equivalent level of expression as that of wild type. Then, we added two other cysteine residues at 137 and 138 to be assessed for the mutation. As a result, the two septet mutations at either cysteines 76/90/138/139/147/149/221 or 76/90/137/139/147/149/221 and the octet mutations at cysteine residues 76/90/137/138/ 139/147/149/221 did not seriously decrease the expression level when compared with the wild type. However, the nine mutations at cysteine residues 76/90/107/137/138/139/147149/221, which include the additional mutation at 107, showed decreased levels of the secreted BNCs that were less than 50% of the wild type by EIA. These results suggest that the eight cysteine residues are probably not essential for the formation and secretion of BNCs.

In Fig. 4, all of the L-BNCs that have multiple mutations were subjected to Western blotting analysis under reducing conditions. The pattern of the derivative L-proteins did not change in the double to octet mutants (Fig. 4, lanes 2 to 10). The band of gpL50 appeared, in contrast to the disappearing gpL44, due to the mutation of cysteine residues 147 and/or 149. These results indicate that substitution of the eight cysteine residues should be effective in producing BNCs, which will lead to avoiding unwanted disulfide bridging.

To compare the sensitivity to DTT of wild type L-BNC and the octet mutant 76/90/137/138/139/147/149/221 (Lm8-) BNC, both BNCs were treated with various concentrations of DTT at 25 °C, and analyzed by SDS-PAGE. The Lm8-protein was about 10 times more sensitive to DTT than was the L-protein (Fig. 5A). To assess the effect of oxidation on both BNCs, L-BNCs and Lm8-BNCs were oxidized by vigorous agitation for various periods and analyzed on SDS-PAGE in the presence of 1 mM DTT (Fig. 5B). The Lm8-protein resisted oxidation for up to 1 min, whereas the L-protein showed little resistance to oxidation (Fig. 5C). The time for the 50% decrease of protein by oxidation was about 10 s in the case of L-BNC while it was around 40 s for Lm8-BNC. These differences in sensitivity to reduction and oxidation between the BNCs might be explained by the number of resultant disulfide bridges due to the replacement of cysteine residues.

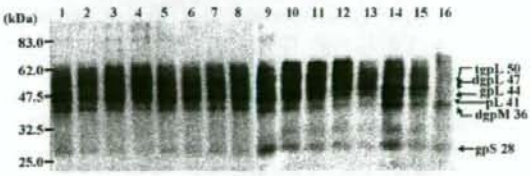

Fig. 4. Analysis of the L-proteins with multiple substitutions at cysteine residues. The wild type and multiple mutant BNCs (Lanes 1 and 9, wild type; lane 2, C/76,90/A; lane 3, C/90/A, C/139/S; lane 4, C/90,147/A; lane 5, C/90,149/A; lane 6, C/90,221/A; lane 7, C/76,90,221/A; lane 8, C/76,90,149,221/A; lane 10, C/76,90,149,221/A, C/139/S; lane 11, C/76,90,147,149,221/A; lane 12, C/76,90,147,149,221/A, C/139/S; lane 13, C/76,90,147,149,221/A, C/138,139/S; lane 14, C/76,90,147,149,221/A, C/137,139/S; lane 15, C/76,90,147,149,221/A, C/137,138,139,S; lane 16, C/76,90,107,147,149,221/A, C/137,138,139/S) were transiently expressed in COS7 cells and were immunoprecipitated and analyzed by Western blotting as described in Fig. 2. The arrows indicate the position of glycosylated (gpS 28) S-protein, diglycosylated (dgpM 36) M-protein, glycosylated (gpL 44), diglycosylated (dgpL 47), and triglycosylated (tgpL50) L-protein.

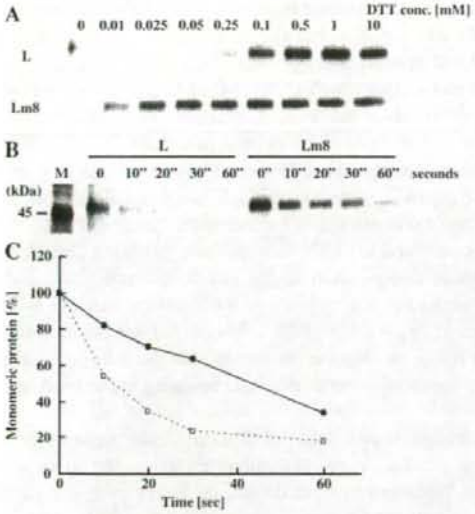

Fig. 5. Sensitivity to redox conditions of wild type and Lm8 BNCs. (A), the BNCs purified from yeast cells were treated with various concentrations of DTT for 10 min at 25 °C and analyzed on SDS-PAGE. For the reference of total amount, the L-protein treated with 10 mM DTT was boiled prior to SDS-PAGE. (B), the effect of oxidation on the BNCs was assessed. The wild type L-and Lm8-protein were analyzed in the presence of 1 mM DTT by SDS-PAGE. The protein bands were made visible by silver staining. Lane M, ovalbumin (molecular weight marker at 45 kDa). (C), resistance against oxidization. The bands of L-and Lm8-protein in (B) were densitometorically analyzed by Image J. Based on the density, the time course change of the amount of monomeric proteins was plotted. The amount at time 0 is taken as 100% for each protein. Solid circle depicts Lm8-BNC and open square depicts L-BNC.

4.3. Conformation of Lm8-protein compared with L-protein

Since the primary sequence of envelope protein contains several potential trypsin cleavage sites, consisting of Arg and Lys in the surface region of the BNCs, fragments cleaved with trypsin could possibly differ if there is a significant difference in the topology between these proteins. To determine if there is a difference of topological structures between L- and Lm8-proteins, the same amount of L- and Lm8-BNCs were digested with various concentrations of trypsin and analyzed by Western blotting (Fig. 6A). As a result, the three major fragments of Trs, Trl, and gTr at 24, 25, and 27 kDa respectively, were observed in both BNCs. It was noted that there was little significant structural difference between L- and Lm8-protein in the BNC due to the mutation. However, Lm8-BNC was resistant to trypsin at the concentration of 1.5 ng/ml, while the wild type L-BNC was digested at 0.75 ng/ml. Furthermore, digestion of Lm8-BNC showed that the major tryptic fragment was gTr, while Trl and Trs were apparent in the digestion of wild type L-BNCs. When treated

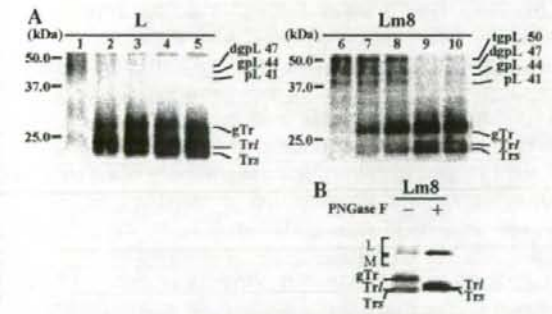

Fig. 6. Comparison of the topology of wild type L-and Lm8-BNCs by trypsin. After each BNC of the same EIA value was immunoprecipitated (A) the BNCs of wild type (lane 1to 5) and Lm8 (lane 6 to 10) were incubated with trypsin (lanes 2 to 5 and 7 to 10) or without trypsin (lanes 1 and 6) for an hour at 37 °C. The digested fragments were detected by Western blotting using anti-S antibodies. These BNCs were digested with various concentration of trypsin at 0.75 ng/ml (lane 2, 7), 1.5 ng/ml (lane 3, 8), 3 ng/ml (lane 4, 9), 6 ng/ml (lane 5, 10). (B) The BNCs of Lm8 were incubated with trypsin and treated with (left) or without (right) glycosidase F (PNGase F). The degraded tryptic fragments were observed to be glycosylated fragments (gTr), non-glycosylated short fragments (Trs) and large fragments (Trl).

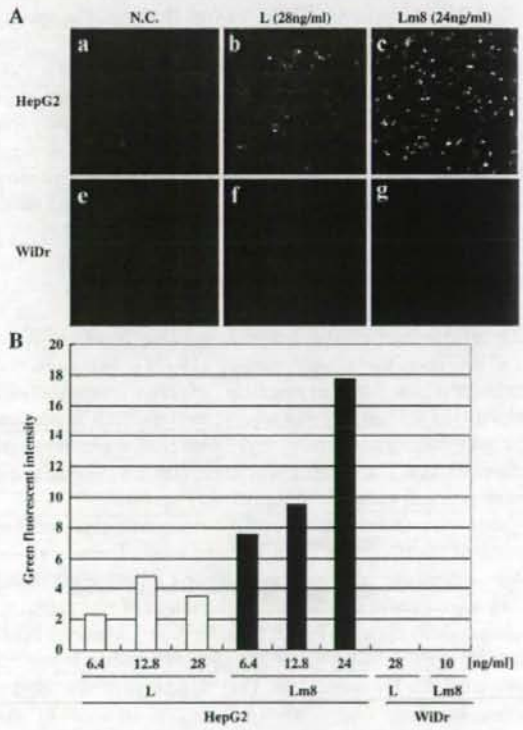

Fig. 7. (A) Gene transduction with wild type L-and Lm8-BNCs. The BNCs incorporating GFP expression vectors were infected into the human hepatocarcinoma-derived HepG2 cells (a, b, c d) and human colon adenocarcinoma-derived WiDr cells (e, f, g, h). GFP expression vector (500 ng) mixed with either wild type BNCs (28 ng/ml) or Lm8-BNCs (24 ng/ml) was subjected to electroporation and added to the culture media of each cell line (b, f and c, g, respectively). As a control for background, only GFP expression vector (500 ng) without any BNCs was added to the media (a, b). Cells were observed for fluorescence on day 3 following addition under a confocal laser scanning microscope. The magnification is ×20. (B) Comparison of infectious efficiency between L-BNC and Lm8-BNC. The images of cells expressing GFP obtained from the confocal laser scanning microscope were analyzed for green color intensity by RGB histogram in Image J. Cells were equally distributed in each field of microscopic observation.(For interpretation of the references to colour in this figure legend, the reader is referred to the web version of this article.)

with *N*-glycosidase F after digestion of both BNCs by trypsin, gTr was found to be degraded to Trs or Trl, so that gTr was implied as the *N*-glycosylated form of Trs or Trl (Fig. 6B) [18]. Lm8-protein should cause the glycosylation attachment site to be more accessible than the wild type. These results suggest that the structure of Lm8-BNC should differ in critical aspects from that of L-BNC.

4.4. Lm8-BNC targeting to HepG2 cells

The potential of Lm8-BNC as a vector specific to human liver cells was evaluated by comparison with L-BNC. An infection experiment was carried out on both human hepatoma-derived HepG2 cells and human colon adenocarcinoma-derived WiDr cells. The L- and Lm8-BNCs incorporated GFP expression plasmid were added into the culture media of these cells. Three days after infection, the cells were observed for GFP fluorescence. Both L-and Lm8-BNCs showed fluorescence, specifically in HepG2 cells, whereas no expression of GFP was observed in WiDr cells incubated with either BNC (Fig. 7). Furthermore, Lm8-BNCs appeared to show more expression of GFP in HepG2 cells than L-BNC of the same amount. The analysis of the images obtained by confocal microscope showed the increase of green fluorescence in a dose dependent manner. The greater the amount of Lm8-BNC that was used, the more expression of GFP in HepG2 cells was shown.

5. Discussion

The significance of the fourteen cysteine residues of L-protein has been extensively studied [19–21]. However, the essential residues for the assembly of HBV particles still remained to be studied. In this study, we explored how to prepare BNCs with enhanced stability by optimizing the number of cysteine residues. The ultimate objective is the development of a far more efficient vector for drug delivery systems.

When each cysteine residue at 48, 65 and 69 was replaced, the secretion of the BNC was not detectable at all. These cysteine residues, which are only conserved among all hepadnaviruses [22,23], appear indispensable for the secretion of vial particles. As schematically drawn in Fig. 2, these three residues are located inside of the BNC and present in the cytoplasm when L-protein is integrated into the membrane. They appear to hardly form a disulfide bridging due to the reducing conditions of the cytoplasm. They might be involved in some significant function such as palmitoylation, often found in the juxtamembranous cysteine residues in viral glycoproteins. Replacement of the cysteine residues present at the cytoplasmic side in the envelope has been reported to prevent the budding and infection of sindbis virus and human immunodeficiency virus [24]. This might be also the case with HBV.

Mutation of cysteine residue at either 121 or 124 significantly decreased the secretion of the BNC down to the same level as those of the mutations at the three internal residues described above. Since these two cysteine residues are located in the outer surface hydrophilic region of the S domain, they are possibly involved in the essential disulfide bridging [19,25]. Cys121 is considered to be involved in the intra-molecular disulfide bond, not only with Cys124, but also with Cys147 [21]. On the other hand, Cys124 is reported to bind with Cys137 [26].

The mutations at 76, 90, 139, 147, 149 and 221 did not show drastic decreases in the level of secretion. The mutations at 107, 137 and 138 showed slight decreases, but not less than 50% of the secretion of wild type BNCs, although the mutation of one or two of these cysteine residues has been described to be essential for secretion [27]. Furthermore, cysteine residue at 221 is not conserved in HBV subtype adw, showing that cysteine residues at this position might not be essential [28]. Taking these results into consideration, we assumed that the cysteine residues at 76, 90, 139, 147, 149 and 221 are not essential to form a BNC, leaving the possibility that those at 107, 137 and 138 are involved in some disulfide bridging in the formation of BNC.

To design more stable BNCs, multiple replacements of cysteine residue were evaluated. Even in the BNCs with multiple replacement from double up to sextuple, the secreted amount of the BNCs was almost equivalent to that of the wild type L-BNC. The sextuple mutant was subjected to further replacement of cysteine residues at each position of 107, 137 and 138. Interestingly, the replacement of the seventh cysteine residues at both 137 and 138 did not change the secretion level, so that the secreted level of the octet mutation, including both of these two, was 80% of wild type L-BNC. However, the ninth mutation at 107 showed a significant decrease of secretion, which was lower than 50% of wild type L-BNC. In contrast, it was previously reported that the simultaneous replacement of cysteine residues at 107, 137 and 138 show an inhibitory effect on the secretion of subviral particles [27]. Taking this into consideration, the cysteine residue at 107 should be essential for the secretion of BNCs. Finally, we obtained Lm8-BNCs, which have the eight cysteine residues replaced. The Lm8-BNCs were more sensitive to reducing reagent and less sensitive to oxidation than L-BNCs. This implied that Lm8-BNCs should be free from false disulfide linking. When the BNCs were expressed in COS7 cells, the glycosylation site appeared to be more accessible in Lm8-protein than in wild type L-protein. This suggests that the site is open without unessential cross-linking between the cysteine residues. This open structure should be created by the replacement of two cysteine residues at 147 and 149, thereby enhancing the accessibility of the enzyme responsible for the glycosylation at Asn146 [18,29,30]. Although the roles of glycosylation in HBV are not yet clear, there have been several reports that describe *N*-linked glycosylation as necessary for virion secretion [31], for reduction of the viral antigenicity and for resistance against proteolytic degradation [32]. This glycosylation might be associated with the resistance to trypsin that was acquired in Lm8-BNCs when compared to L-BNCs. The glycosaccharide moiety might make the proteases inaccessible to its recognition site. It is also conceivable that Lm8-protein might acquire stability with less false disulfide bridging, which would result in the denatured state accessible for proteases.

When Lm8-BNC was assessed as a gene transduction vector, the cell type specific GFP expression was successfully observed

in a dose-dependent manner of the BNC (Fig. 7). The gene transduction efficiency by Lm8-BNC was more than two-fold when compared with that by L-BNC. L-BNC itself did not show any cytotoxic activity [15] so that the replacement of cysteine residues should not be related with the decrease of toxic events. The increased efficiency of gene transduction may be due to the enhanced stability of the L-BNC caused by the removal of unessential disulfide bridging. A reason for this is that proteases on the cell surface may degrade the BNC at the infection [33,34]. Degradation of the sequence including hepatocyte recognition site present in PreS1 would seriously impairs the attachment of BNC to hepatocytes [10,17,35] and result in low efficiency of internalization. There might also be an advantage to Lm8-BNC to have pores opened to incorporate substances into the BNCs with less disulfide bridging. One of the biggest hurdles in gene therapy is finding a safe and effective delivery vehicle. Several viral delivery mechanisms are efficient at gene transfer, but pose manufacturing and safety problems. Non-viral vectors are easier to manufacture and often safer but are not as effective. BNC offers tissue specificity and efficiency of a viral approach without the harmful side effects [36]. In this paper, BNC is successfully sophisticated as Lm8-BNC with impaired stability.

6. Conclusion

In this study, we successfully engineered Lm8-BNCs, eliminating unessential disulfide linkages to confer the stability necessary for a delivery vector with enhanced efficiency of gene transduction. This stability is explained by the hyper-glycosylation and by the decreased opportunity of false disulfide links, both of which would prevent the accessibility of proteases. Due to the stability the efficiency of transduction should be enhanced simultaneously. The minimized number of disulfide links, which would not allow the unnecessary intermolecular bonds between L-proteins, will confer the mobility of the components of BNCs showing the enhanced efficiency of gene encapsulation by electroporation. This design of Lm8-BNC should be further applicable to other engineered BNCs, which are expected to appear in the future, such as those devised for protein delivery vector described by Yu et al [37].

Acknowledgments

The authors thank Mr. Nobuhiro Nagatomo, Mr. Tomonori Yabuki and Ms. Kumiko Soga for their excellent technical assistance. Fukuda, T. was supported by the fellowship from Katayama Chemicals Ind. Co. Ltd. This project is partly supported by the Grants-in-Aid from the Japan Science and Technology Corporation (Research Fund for Patenting) and the Ministry of Education, Culture, Sports, Science and Technology, Japan.

References

[1] A. Donsante, C. Vogler, N. Muzyczka, J.M. Crawford, J. Barker, T. Flotte, T.M. Campbell, T. Daly, M.S. Sands, Observed incidence of tumorigenesis in long-term rodent studies of rAAV vectors, Gene Ther. 8 (17) (2001) 1343–1346.

[2] K. Lundstrom, Latest development in viral vectors for gene therapy, Trends Biotechnol. 21 (3) (2003) 117–122.

[3] A.D. Miller, The problem with cationic liposome/micelle-based non-viral vector systems for gene therapy, Curr. Med. Chem. 10 (14) (2003) 1195–1211.

[4] X. Fu, X. Zhang, Delivery of herpes simplex virus vectors through liposome formulation, Molec. Ther. 4 (5) (2001) 4447–4453.

[5] Y. Kaneda, New vector innovation for drug delivery: development of fusigenic non-viral particles, Curr. Drug Targets 4 (8) (2003) 599–602.

[6] M. Mizuno, Y. Ryuke, J. Yoshida, Cationic liposomes conjugation to recombinant adenoviral vectors containing herpes simplex virus thymidine kinase gene followed by ganciclovir treatment reduces viral antigenicity and maintains antitumor activity in mouse experimental glioma models, Cancer Gene Ther. 9 (10) (2002) 825–829.

[7] Y. Fujisawa, S. Kuroda, P.M.C.A. Van Eerd, H. Schellekens, A. Kakinuma, Protective efficacy of a novel hepatitis B vaccine consisting of M (pre-S2+S) protein particles (a third generation vaccine), Vaccine 8 (3) (1990) 192–198.

[8] V. Bruss, R.J. Thomssen, Mapping a region of the large envelope protein required for hepatitis B virion maturation, J. Virol. 68 (3) (1994) 1643–1650.

[9] J. Le Seyec, P. Chouteau, I. Cannie, C. Guguen-Guillouzo, P. Gripon, Role of the pre-S2 domain of the large envelope protein in hepatitis B virus assembly and infectivity, J. Virol. 72 (7) (1998) 5573–5578.

[10] A.R. Neurath, S.B. Kent, N. Strick, K. Parker, Identification and chemical synthesis of a host cell receptor binding site on hepatitis B virus, Cell 46 (3) (1986) 429–436.

[11] A.R. Neurath, B. Seto, N. Strick, Antibodies to synthetic peptides from the preS1 region of the hepatitis B virus (HBV) envelope (env) protein are virus-neutralizing and protective, Vaccine 7 (3) (1989) 234–236.

[12] M.A. Petit, F. Capel, S. Dubanchet, H. Mabit, PreS1-specific binding proteins as potential receptors for hepatitis B virus in human hepatocytes, Virology 187 (1) (1992) 211–222.

[13] T. Yamada, H. Iwabuki, T. Kanno, H. Tanaka, T. Kawai, H. Fukuda, A. Kondo, M. Seno, K. Tanizawa, S. Kuroda, Physicochemical and immunological characterization of hepatitis B virus envelope particles exclusively consisting of the entire L (pre-S1+pre-S2+S) protein, Vaccine 19 (23–24) (2001).

[14] S. Kuroda, S. Otaka, T. Miyazaki, M. Nakao, Y. Fujisawa, Hepatitis B virus envelope L-protein particles. Synthesis and assembly in *Saccharomyces cerevisiae*, purification and characterization, J. Biol. Chem. 267 (3) (1992) 1953–1961.

[15] T. Yamada, Y. Iwasaki, H. Tada, H. Iwabuki, M.K. Chuah, T. VandenDriessche, H. Fukuda, A. Kondo, M. Ueda, M. Seno, K. Tanizawa, S. Kuroda, Nanoparticles for the delivery of genes and drugs to human hepatocytes, Nat. Biotechnol. 21 (8) (2003) 885–890.

[16] M. Kobayashi, T. Asano, M. Utsunomiya, Y. Itoh, Y. Fujisawa, O. Nishimura, K. Kato, A. Kakinuma, Recombinant hepatitis B virus surface antigen carrying the pre-S2 region derived from yeast: purification and characterization, J. Biotechnol. 8 (1) (1988) 1–22.

[17] J. Le Seyec, P. Chouteau, I. Cannie, C. Guguen-Guillouzo, P. Gripon, Infection process of the hepatitis B virus depends on the presence of a defined sequence in the pre-S1 domain, J. Virol. 73 (3) (1999) 2052–2057.

[18] R. Prange, R.E. Streeck, Novel transmembrane topology of the hepatitis B virus envelope proteins, EMBO J. 14 (2) (1995) 247–256.

[19] B.A. Antoni, I. Rodriguez-Crespo, J. Gomez-Gutierrez, M. Nieto, D. Peterson, F. Gavilanes, Site-directed mutagenesis of cysteine residues of hepatitis B surface antigen. Analysis of two single mutants and the double mutant, Eur. J. Biochem. 222 (1) (1994) 121–127.

[20] C.M.T. Mangold, R.E. Streeck, Mutational analysis of the cysteine residues in the hepatitis B virus small envelope protein, J. Virol. 67 (8) (1993) 4588–4597.

[21] C.M.T. Mangold, F. Unckell, M. Werr, R.E. Streeck, Analysis of intermolecular disulfide bonds and free sulfhydryl groups in hepatitis B surface antigen particles, Arch. Virol. 142 (11) (1997) 2257–2267.

[22] F. Galibert, T.N. Chen, E. Mandart, Nucleotide sequence of a cloned woodchuck hepatitis virus genome: comparison with the hepatitis B virus sequence, J. Virol. 41 (1) (1982) 51–65.

[23] H. Norder, B. Hammas, S. Lofdahl, A.M. Courouce, L.O. Magnius, Comparison of the amino acid sequences of nine different serotypes of

hepatitis B surface antigen and genomic classification of the corresponding hepatitis B virus strains, J. Gen. Virol. 73 (Pt5) (1992) 1201–1208.

[24] I. Rousso, M.B. Mixon, B.K. Chen, P.S. Kim, Palmitoylation of the HIV-1 envelope glycoprotein is critical for viral infectivity, Proc. Natl. Acad. Sci. U. S. A. 97 (25) (2000) 13523–13525.

[25] Y.C. Chen, K. Delbrook, C. Dealwis, L. Mimms, I.K. Mushahwar, W. Mandecki, Discontinuous epitopes of hepatitis B surface antigen derived from a filamentous phage peptide library, Proc. Natl. Acad. Sci. U. S. A. 93 (5) (1996) 1997–2001.

[26] T. Koyanagi, M. Nakamuta, H. Sakai, R. Sugimoto, M. Enjoji, K. Koto, H. Iwamoto, T. Kumazawa, M. Mukaide, H. Nawata, Analysis of HBs antigen negative variant of hepatitis B virus: unique substitutions, Glu129 to Asp and Gly145 to Ala in the surface antigen gene, Med. Sci. Monit. 6 (6) (2000) 1165–1169.

[27] C.M.T. Mangold, F. Unckell, M. Werr, R.E. Streeck, Secretion and antigenicity of hepatitis B virus small envelope proteins lacking cysteines in the major antigenic region, Virology 211 (2) (1995) 535–543.

[28] H. Okamoto, F. Tsuda, H. Sakugawa, R.I. Sastrosoewignjo, M. Imai, Y. Miyakawa, M. Mayumi, Typing hepatitis B virus by homology in nucleotide sequence: comparison of surface antigen subtypes, J. Gen. Virol. 69 (Pt10) (1988) 2575–2583.

[29] A. Mehta, X. Lu, T.M. Block, B.S. Blumberg, Hepatitis B virus (HBV) envelope glycoproteins vary drastically in their sensitivity to glycan processing: evidence that alteration of a single *N*-linked glycosylation site can regulate HBV secretion, Proc. Natl. Acad. Sci. U. S. A. 94 (5) (1997) 1822–1827 (R.A. Dwek).

[30] H. Loffler-Mary, M. Werr, R. Prange, Sequence-specific repression of cotranslational translocation of the hepatitis B virus envelope proteins coincides with binding of heat shock protein Hsc70, Virology 235 (1) (1997) 144–152.

[31] X. Lu, A. Mehta, R. Dwek, T. Butters, T. Block, Evidence that *N*-linked glycosylation is necessary for hepatitis B virus secretion, Virology 213 (2) (1995) 660–665.

[32] J. Lee, J.S. Park, J.Y. Moon, K.Y. Kim, H.M. Moon, The influence of glycosylation on secretion, stability, and immunogenicity of recombinant HBV pre-S antigen synthesized in *Saccharomyces cerevisiae*, Biochem. Biophys. Res. Commun. 303 (2) (2003) 427–432.

[33] D. Glebe, W.H. Gerlich, Study of the endocytosis and intracellular localization of subviral particles of hepatitis B virus in primary hepatocytes, Methods Mol. Med. 96 (2004) 143–151.

[34] X. Lu, T.M. Block, W.H. Gerlich, Protease-induced infectivity of hepatitis B virus for a human hepatoblastoma cell line, Virology 70 (4) (1996) 2277–2285.

[35] P. Pontisso, F. Galabrese, L. Benvegnu, M. Lise, C. Belluco, M.G. Ruvoletto, M. Marino, M. Valente, D. Nitti, A. Gatta, G. Fassina, Overexpression of squamous cell carcinoma antigen variants in hepatocellular carcinoma, Br. J. Cancer 90 (4) (2004) 833–837.

[36] D. Lawrence, Nanotechnology takes another small step forward, Lancet 362 (2003) 48.

[37] D. Yu, C. Amano, T. Fukuda, T. Yamada, S. Kuroda, K. Tanizawa, A. Kondo, M. Ueda, H. Yamada, H. Tada, M. Seno, The specific delivery of proteins to human liver cells by engineered bio-nanocapsules, FEBS J. 272 (14) (2005) 3651–3660.

J Neurosurg 106:1070–1074, 2007

Use of 5-aminolevulinic acid in fluorescence-guided resection of meningioma with high risk of recurrence

Case report

YOSHINAGA KAJIMOTO, M.D., PH.D.,[1] TOSHIHIKO KUROIWA, M.D., PH.D.,[1] SHIN-ICHI MIYATAKE, M.D., PH.D.,[1] TSUGUMICHI ICHIOKA, M.D., PH.D.,[1] MINORU MIYASHITA, M.D.,[1] HIDEKAZU TANAKA, M.D.,[1] AND MOTOMU TSUJI, M.D., PH.D.[2]

Departments of [1]Neurosurgery and [2]Surgical Pathology, Osaka Medical College, Osaka, Japan

✓It has been established that fluorescence-guided resection using 5-aminolevulinic acid (5-ALA) is useful in glioma surgery. The authors report on a 65-year-old woman who had a huge atypical left-hemisphere meningioma, which extended into the skull and to the superior sagittal sinus and demonstrated fluorescence in response to administration of 5-ALA. After the tumor was removed, the operative field was observed under the fluorescent mode of a fluorescence surgical microscopy system. Several minute areas of residual tumor tissue were visualized as strong fluorescence behind the vein and sinus, in a part of the hypertrophic dura, and along the edge of the skull. These remnants were completely removed. The authors concluded that fluorescence-guided resection using 5-ALA is useful in cases of atypical meningiomas with a high risk of recurrence.

KEY WORDS • **meningioma** • **5-aminolevulinic acid** • **photodynamic diagnosis** • **fluorescence-guided resection**

RECENT advances in fluorescence diagnostic technology make it easier to reliably achieve complete excision of malignant gliomas.[22,24] Gross-total resection has been shown to prolong the survival time of glioblastoma patients.[12,20,22] Historically, two fluorescent agents, fluorescein sodium[11,20] and 5-ALA,[13,22,23] have been used in glioma surgery. Because of its high tumor specificity and safety, 5-ALA is particularly promising. It actively accumulates in the neoplasm and is converted to PPIX, which is fluorescent.[16,24] This phenomenon has been clinically applied to the detection of neoplasms in the brain and other organs, such as the bladder, skin, and bronchus. Therefore, this technique is generally termed fluorescence diagnosis or photodynamic diagnosis.

In the past 2 years, we also have performed fluorescence-guided tumor resection using 5-ALA,[13] and we have found a marked improvement in the percentage of tumor tissue we were able to resect. In our experience, not only malignant gliomas but almost all meningiomas have shown bright fluorescence in response to administration of 5-ALA. Because meningiomas are usually benign and well circumscribed, there is generally little need for fluorescence guidance during surgical treatment of these lesions. Occasionally, however, the lesions become malignant and/or invade important surrounding structures, such as vessels, dura mater, bone, and brain, especially at recurrence. When such invasion occurs, it is common for some tumor remnants to go unnoticed and lead to recurrence.[6–8] Therefore, fluorescence-guided resection may be beneficial for the removal of complicated or malignant meningiomas that have a high risk of recurrence.

Abbreviations used in this paper: PPIX = protoporphyrin IX; MR = magnetic resonance; 5-ALA = 5-aminolevulinic acid;

Case Report

History and Presentation. This 65-year-old right-handed woman presented with a 1-month history of progressing right-sided motor weakness and headache.

Examination. An MR imaging study of the brain revealed a huge meningioma (maximum diameter 7 cm) at the left frontal convexity, extending to the superior sagittal sinus and skull and causing the skull to bulge (Fig. 1A). The tumor had a lobular shape and completely surrounded a cortical vein. The adjacent brain parenchyma was edematous and extremely distorted. At the dural attachment, hypertrophy of the dura mater, the so-called dural tail sign, was identified.

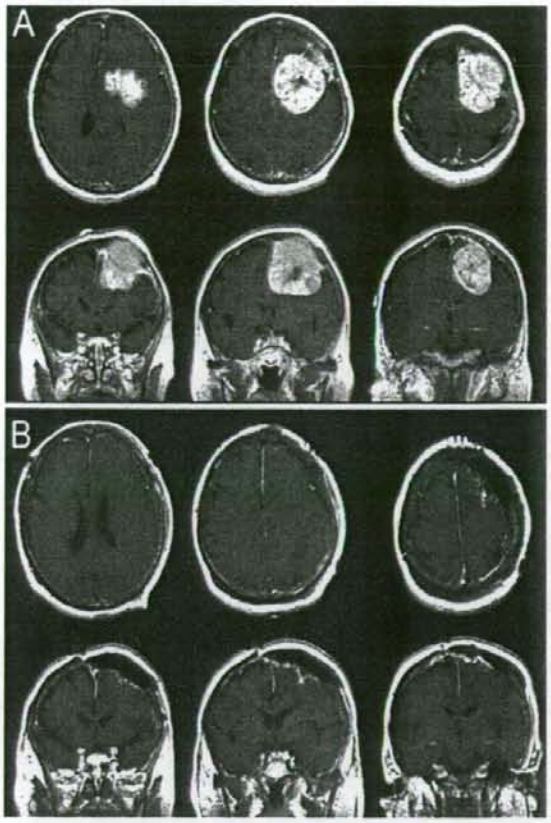

FIG. 1. Gadolinium-enhanced T_1-weighted MR images. A: Preoperative images showing the large tumor with a dural tail sign that reached the superior sagittal sinus. Skull invasion is evident. B: Postoperative images obtained 24 hours after surgery. No enhancing lesion related to the meningioma was observed.

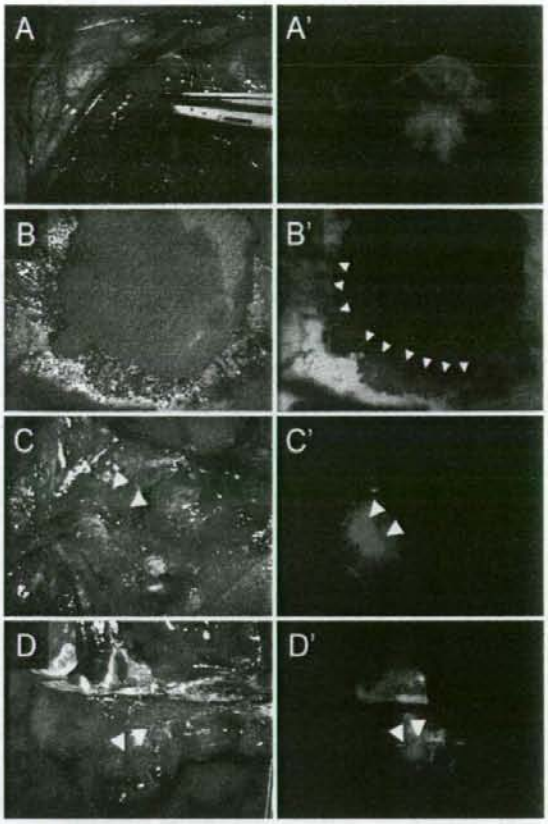

FIG. 2. Intraoperative photographs obtained in the white-light mode (A, B, C, D) and in the fluorescence mode (A′, B′, C′, D′). All images were obtained using a fluorescence surgical microscope. Each set of corresponding images (A and A′, B and B′, C and C′, D and D′) shows a single field of view. A and A′: The main tumor mass showed bright fluorescence. B and B′: The edge of the resected bone showed multiple areas of fluorescence. C and C′: A small area of residual tumor was identified by fluorescence behind the cortical vein. D and D′: Hypertrophic dura mater *(arrowheads)* adjacent to the superior sagittal sinus demonstrated fluorescence activity due to tumor invasion.

Operation. Resection of the lesion was carried out via a frontal craniotomy using a fluorescence microscopy system consisting of an ordinary surgical microscope (Carl Zeiss), an excitation light source (D-Light, Carl Storz), a fluorescence filter (Wratten No. 12, Kodak), and an electric filter changer integrated with the microscope. (This system allows the surgeon to observe the operative field using either the ordinary white-light mode or the fluorescence mode and change between these modes instantly.)

Three hours before the operation, 20 mg/kg of 5-ALA was administered orally. At the early stage of the surgical procedure, we confirmed that the tumor showed the bright charcoal red fluorescence of PPIX in the fluorescence mode (Fig. 2A and A′). We performed gross-total resection of the mass under white-light illumination, and then searched for and explored residual tumor in the fluorescence mode.

Some tumor remnants were identified by strong fluorescent areas in an obscure sulcus and behind the cortical vein (Fig. 2C and C′) that had been completely encased in tumor before resection, and other remnants were visible behind the venous lake and superior sagittal sinus. Some portions of the hypertrophic dura mater were visualized as bright fluorescent layers (Fig. 2D and D′), but no fluorescence was observed in most parts of the widespread hypertrophic areas of the dura.

Guided by fluorescence, we excised the convexity dura using a margin of 10 mm from the tumor except adjacent to the superior sagittal sinus. Tumor invasion into the skull flap was also clearly visualized by the fluorescence (Fig. 2B and B′). The skull flap was drilled out until no more tumor fluorescence was visible. Closure was achieved using an artificial bone flap made of resin.

Postoperative Imaging and Histological Findings. Postoperative MR imaging revealed no abnormally enhanced lesion related to the residual tumor, except on the adjacent gliotic brain tissue (Fig. 1B).

The histopathological diagnosis of the main tumor mass was atypical meningioma (Fig. 3A); the tumor's MIB-1 in-

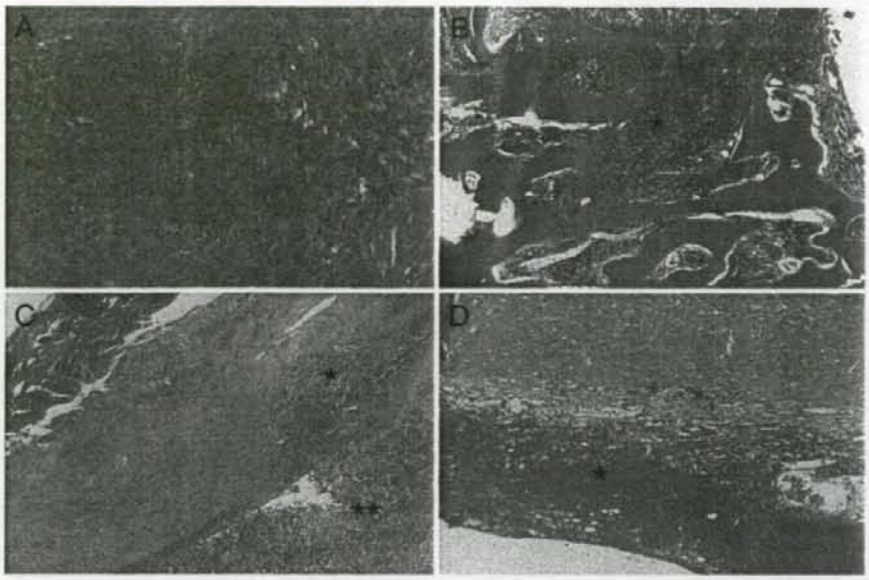

FIG. 3. Photomicrographs demonstrating histological findings. A: Main tumor mass. B: Tumor invasion *(asterisk)* into the skull. C: Hypertrophic dura mater showing 5-ALA–induced fluorescence. *Asterisk* indicates fluorescence-positive tumor invasion into dura mater; *double asterisk* indicates intradural tumor mass. D: Hypertrophic dura without 5-ALA–induced fluorescence. *Asterisk* indicates venous congestion. No tumor invasion was observed. H & E. Original magnifications × 100 (A) and × 20 (B, C, and D).

dex reached 5%. Specimens from all areas of the strongly fluorescent surrounding tissue, which consisted of bone and hypertrophic dura, were confirmed to contain tumor cell clusters (Fig. 3B and C). In samples of neighboring tissue without fluorescence, no tumor cells were detected (Fig. 3D).

Postoperative Course. Within a week after the operation, the patient's symptoms were completely resolved. At the latest follow-up examination, 2.5 years after surgery, there was still no evidence of recurrence.

Discussion

Although fluorescent PPIX accumulates selectively in numerous neoplasms, its accumulation in the normal central nervous system is restricted except in the subependymal zone and choroid plexus.[4,15] We observed that the dura mater and the arachnoid membrane showed no PPIX fluorescence but strong green autofluorescence. These tissues were, however, the meningioma's sites of origin. Many possible mechanisms have been posited to explain the selective accumulation of PPIX in neoplasm: enhanced tissue penetration of 5-ALA, increased intracellular uptake, accelerated activity of plasma enzymes involved in the synthesis of intermediates for PPIX, and reduced activity of ferrochelatase, which converts PPIX to heme.[16] At least one of these factors is probably involved in the strong 5-ALA–derived fluorescence in meningiomas. In general, there is no strict correlation between cell proliferation and PPIX accumulation. In meningiomas, the proliferation rate is relatively low.[5] In our series of meningioma cases in which we used photodynamic diagnosis, 5-ALA administration resulted in bright and diffuse tumor fluorescence in 20 (83%) of 24 cases, including the cases in which preoperative embolization had been performed (Table 1). No relationship was found between degree of malignancy and tumor fluorescence. We observed PPIX fluorescence only in the main mass and areas of tumor invasion. In this series, the sensitivity and specificity of PPIX fluorescence of main tumor mass were 83% (20 of 24 cases) and 100% (20 of 20 cases), respectively (Table 1).

Fluorescence observation allowed us to identify the extent of the tumor and helped us to avoid leaving residual tumor tissue that was difficult to identify in the white-light mode. If we had not employed fluorescence guidance, we might not have noticed several small areas of residual tumor.

In the case presented in this article, numerous factors influenced the recurrence of the tumor: the atypical meningioma histological type, the tumor's moderately high MIB-1 index, and its soft consistency, lobular shape, and dural attachment very close to the venous sinus, as well as bone invasion. Because of these factors the risk of recurrence was considered very high.[1,6,7,14] It is worth noting that the tumor remnants were identified by fluorescence in multiple regions. Philippon and Cornu[17] and deVries and Wakhloo[3] have reported that recurrent tumor is often found at multiple sites. Meningioma has a high risk of recurrence, and during excision meningioma tissue can be left at any attachment to surrounding tissues, especially at attachments to the gliotic brain, major sinuses, the anterior visual pathway,[21] and marginal dura mater. Aggressive excision of the dura and gliotic brain has been recommended to reduce this risk,[14,19] but the optimal extent of dural resection has been

TABLE 1

*Meningioma fluorescence induced by administration of 5-ALA**

Case No.	Age (yrs), Sex	Tumor Location	WHO Grade	Tumor Fluorescence	Preop Embolization†
1	54, F	intraosseous	I	none	no
2	56, M	sphenoid ridge	II	none	no
3	63, M	convexity	I	none	no
4	56, M	internal meatus	I	none	no
5	62, F	convexity	III	strong	no
6	49, F	convexity	I	strong	no
7	66, F	parasagittal	I	strong	no
8	60, F	parasagittal	III	strong	no
9	69, M	falx	II	strong	no
10	51, F	sphenoid wing	I	strong	no
11	39, F	convexity	I	strong	no
12	65, F	parasagittal	II	strong	no
13	34, M	convexity	I	strong	no
14	64, F	convexity	II	strong	no
15	29, F	parasagittal	I	strong	no
16	46, F	sphenoid ridge	I	strong	no
17	47, F	falx	I	strong	yes
18	73, F	petroclival	I	strong	yes
19	63, F	posterior fossa	I	strong	no
20	69, F	convexity	I	strong	no
21	61, F	parasagittal	I	strong	no
22	71, M	convexity	I	strong	yes
23	51, M	convexity	I	strong	yes
24	73, M	temporal base	I	strong	yes

* WHO = World Health Organization.
† Polyvinyl acetate was used for embolization.

controversial. Borovich and Doron[2] have proposed a 4-cm margin, and Kinjyo and colleagues[10] have proposed a margin of 2 cm. Nakasu et al.[14] have reported that a 1-cm dural margin is not sufficient to prevent recurrence. The most suitable margin for dural excision will necessarily differ from case to case, because of differences in tumor growth rates and invasiveness. In light of these factors, photodynamic diagnosis may become a promising method of determining the extent of dural resection.

On the other hand, indiscriminate excision can lead to complications related to brain and vascular injury. Therefore, if a tumor is located close to a major sinus, the skull base, or an eloquent area, then the excision of dura mater and brain tissue should be restricted to safe areas, and unresectable dura must be coagulated. The application of fluorescence may help to avoid unnecessary excision.

The reasons why tumor remnants may be overlooked can be classified into three categories. 1) The tumor cells invade surrounding tissue, attached dura mater, bone, and brain, after which the invaded area is difficult to distinguish from the noninvaded area (Fig. 4A–C). 2) The tumor remnants may be hidden behind large vessels or the sinus, dural fold, or sulcus (Fig. 4D). 3) Daughter lesions may develop apart from the main mass. All three reasons can make tumor remnants difficult to identify with the naked eye or with the aid of a surgical microscope. The use of 5-ALA–induced fluorescence can help surgeons identify tumor remnants because an area of strong red fluorescence will appear if even a small part of a remnant is present at the tissue surface.

We found that only limited areas of hypertrophic dura mater demonstrated red fluorescence, and these could be clearly distinguished from nontumoral hypertrophic dura using the photodynamic diagnosis technique. Furthermore,

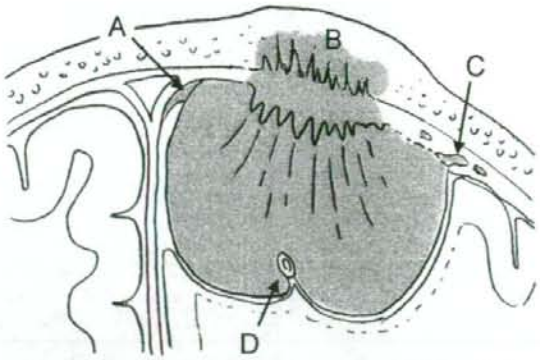

FIG. 4. Schematic drawing showing areas most likely to harbor tumor remnants. A: Intradural invasion. B: Bone invasion. C: Dural extension. D: Tumor tissue behind vessels in the sulcus. The *gray zone* shows the extent of the tumor.

histological analysis showed that hypertrophic dura that manifested red fluorescence included invading tumor tissue, while that without red fluorescence included no tumor tissue (Fig. 3C and D).

Most of the dural tail represents venous congestion. In a case series reported by Kawahara et al.,[9] tumor cells were found to have invaded the dura in only 33% of cases in which the dural tail was evident. Nevertheless, it is difficult to discriminate between tumoral and nontumoral dural hypertrophy during surgery. In eight of our series of meningioma cases in which photodynamic diagnosis was used, dural hypertrophy was revealed by preoperative MR imaging and was evaluated through fluorescence mode observation during surgery (Table 2). In six cases, PPIX fluorescence was present in hypertrophic lesions. Histologically, we confirmed that in five of the six cases, most of the hypertrophic dura mater identified by PPIX fluorescence contained meningioma cells. Therefore, the sensitivity of PPIX fluorescence in hypertrophic dura is 100% (five of five cases), and its specificity is 83% (five of six cases) (Table 2). Fluorescence can make it easy to distinguish the one from the other and determine the extent of a given tumor.

In our case, the tumor's invasion of the skull was also visualized by red fluorescence. In most cases, hyperostosis in association with meningioma is related to tumor invasion.[18] However, the extent of tumor invasion is difficult to judge from appearance alone. Although it is relatively easy to treat bone invasion in cases of convexity meningioma, invasion

TABLE 2

Tumor cell invasion and dural fluorescence in eight patients with dural hypertrophy

Case No.	PPIX Fluorescence	Tumor Cell Invasion
6	yes	yes
11	no	no
12	yes	yes
13	no	no
15	yes	no
20	yes	yes
21	yes	yes
22	yes	yes

at the skull base is hard to treat because it involves the cranial nerves, major blood vessels, and air sinuses. Therefore, the detection of bone invasions using photodynamic diagnostic methods would seem to be valuable, especially in surgery for skull-base meningiomas.

This is the first report of meningioma showing strong red fluorescence in response to administration of 5-ALA. We conclude that applying this method to meningiomas that have a high risk of recurrence should be of value not only in ensuring that tumor remnants are not overlooked during resection but also in helping to avoid unnecessarily radical resection and the associated risk of morbidity. To confirm the usefulness of fluorescence-guided surgery for meningioma, further studies on its sensitivity, specificity, and influence on recurrence rates should be conducted.

Acknowledgments

We are very grateful to Professor Walter Stummer of the Department of Neurosurgery at Heinrich Heine University, Düsseldorf, Germany, for fruitful discussions.

References

1. Al-Mefty O, Kadri PAS, Pravdenkova S, Sawyer JR, Stangeby C, Husain M: Malignant progression in meningioma: documentation of a series and analysis of cytogenetic findings. **J Neurosurg 101:**210–218, 2004
2. Borovich B, Doron Y: Recurrence of intracranial meningiomas: the role played by regional multicentricity. **J Neurosurg 64:** 58–63, 1986
3. de Vries J, Wakhloo AK: Repeated multifocal recurrence of grade I, grade II, and grade III meningiomas: regional multicentricity (primary new growth) or metastases? **Surg Neurol 41:** 299–305, 1994
4. Ennis SR, Novotny A, Xiang J, Shakui P, Masada T, Stummer W, et al: Transport of 5-aminolevulinic acid between blood and brain. **Brain Res 959:**226–234, 2003
5. Iinuma S, Farshi SS, Ortel B, Hasan T: A mechanistic study of cellular photodestruction with 5-aminolevulinic acid-induced porphyrin. **Br J Cancer 70:**21–28, 1994
6. Jääskelainen J: Seemingly complete removal of histologically benign intracranial meningioma: late recurrence rate and factors predicting recurrence in 657 patients. A multivariate analysis. **Surg Neurol 26:**461–469, 1986
7. Jääskelainen J, Haltia M, Servo A: Atypical and anaplastic meningiomas: radiology, surgery, radiotherapy, and outcome. **Surg Neurol 25:**233–242, 1986
8. Kallio M, Sankila R, Hakulinen T, Jääskelainen J: Factors affecting operative and excess long-term mortality in 935 patients with intracranial meningioma. **Neurosurgery 31:**2–12, 1992
9. Kawahara Y, Niiro M, Yokoyama S, Kuratsu J: Dural congestion accompanying meningioma invasion into vessels: the dural tail sign. **Neuroradiology 43:**462–465, 2001
10. Kinjo T, Al-Mefty O, Kanaan I: Grade zero removal of supratentorial convexity meningiomas. **Neurosurgery 33:**394–399, 1993
11. Kuroiwa T, Kajimoto Y, Ohta T: Development of a fluorescein operative microscope for use during malignant glioma surgery: a technical note and preliminary report. **Surg Neurol 50:**41–49, 1988
12. Lacroix M, Abi-Said D, Fourney DR, Gokaslan ZL, Shi W, DeMonte F, et al: A multivariate analysis of 416 patients with glioblastoma multiforme: prognosis, extent of resection, and survival. **J Neurosurg 95:**190–198, 2001
13. Miyatake S, Kuwabara H, Kajimoto Y, Kawabata S, Yokoyama K, Doi A, et al: Preferential recurrence of a sarcomatous component of a gliosarcoma after boron neutron capture therapy: case report. **J Neurooncol 76:**143–147, 2006
14. Nakasu S, Nakasu Y, Nakajima M, Matsuda M, Handa J: Preoperative identification of meningiomas that are highly likely to recur. **J Neurosurg 90:**455–462, 1999
15. Olivo M, Wilson BC: Mapping ALA-induced PPIX fluorescence in normal brain and brain tumor using confocal fluorescence microscopy. **Int J Oncol 25:**37–45, 2004
16. Peng Q, Warloe T, Berg K, Moan J, Kongshaug M, Giercksky KE, et al: 5-aminolevulinic acid-based photodynamic therapy. Clinical research and future challenges. **Cancer 79:**2282–2308, 1997
17. Philippon J, Cornu P: The recurrence of meningiomas, in Al-Mefty O (ed): **Meningiomas.** New York: Raven Press, 1991, pp 87–106
18. Pieper DR, Al-Mefty O, Hanada Y, Buechner D: Hyperostosis associated with meningioma of the cranial base: secondary changes or tumor invasion. **Neurosurg 44:**742–747, 1999
19. Salcman M: Malignant meningiomas, in Al-Mefty O (ed): **Meningiomas.** New York: Raven Press, 1991, pp 75–86
20. Shinoda J, Yano H, Yoshida S, Okumura A, Kaku Y, Iwama T, et al: Fluorescence-guided resection of glioblastoma multiforme by using high-dose fluorescein sodium. Technical note. **J Neurosurg 99:**597–603, 2003
21. Stafford SL, Perry A, Suman VJ, Meyer FB, Scheithauer BW, Lohse CM, et al: Primarily resected meningiomas: outcome and prognostic factors in 581 Mayo Clinic patients, 1978 through 1988. **Mayo Clin Proc 73:**936–942, 1998
22. Stummer W, Novotny A, Stepp H, Goetz C, Bise K, Reulen HJ: Fluorescence-guided resection of glioblastoma multiforme by using 5-aminolevulinic acid-induced porphyrins: a prospective study in 52 consecutive patients. **J Neurosurg 93:**1003–1013, 2000
23. Stummer W, Reulen HJ, Novotny A, Stepp H, Tonn JC: Fluorescence-guided resections of malignant gliomas—an overview. **Acta Neurochir Suppl 88:**9–12, 2003
24. Stummer W, Stocker S, Wagner S, Stepp H, Fritsch C, Goetz C, et al: Intraoperative detection of malignant gliomas by 5-aminolevulinic acid-induced porphyrin fluorescence. **Neurosurgery 42:**518–526, 1998

Manuscript submitted March 22, 2005.
Accepted September 27, 2006.
This work was supported in part by Grants-in-Aid for Scientific Research (C) Nos. 14571345 and 16659396 to Dr. Kuroiwa and Dr. Kajimoto, respectively, and a Grant-in-Aid for Exploratory Research No. 15500351 to Dr. Kuroiwa.

Address reprint requests to: Yoshinaga Kajimoto, M.D., Ph.D., Department of Neurosurgery, Osaka Medical College, 2-7 Daigakumachi, Takatsuki City, Osaka 569-8686, Japan. email: neu039@poh.osaka-med.ac.jp.

BORON NEUTRON CAPTURE THERAPY FOR MALIGNANT TUMORS RELATED TO MENINGIOMAS

Shin-Ichi Miyatake, M.D., Ph.D.
Department of Neurosurgery, Osaka Medical College, Takatsuki City, Japan

Yoji Tamura, M.D., Ph.D.
Department of Neurosurgery, Osaka Medical College, Takatsuki City, Japan

Shinji Kawabata, M.D., Ph.D.
Department of Neurosurgery, Osaka Medical College, Takatsuki City, Japan

Kyoko Iida, M.D.
Department of Neurosurgery, Osaka Medical College, Takatsuki City, Japan

Toshihiko Kuroiwa, M.D., Ph.D.
Department of Neurosurgery, Osaka Medical College, Takatsuki City, Japan

Koji Ono, M.D., Ph.D.
Particle Radiation Oncology Research Center, Research Reactor Institute, Osaka Medical College, Takatsuki City, Japan

Reprint requests:
Shin-Ichi Miyatake, M.D., Ph.D., Department of Neurosurgery, Osaka Medical College, 2-7 Daigaku-machi, Takatsuki City, Osaka, Japan.

Received, July 27, 2006.
Accepted, January 8, 2007.

OBJECTIVE: Malignant meningiomas, similar to glioblastomas, are difficult tumors to control. We tried to control malignant tumors related to meningiomas by boron neutron capture therapy (BNCT).

METHODS: Since June 2005, we applied BNCT with 13 rounds of neutron irradiation to seven cases of malignant tumors related to meningiomas. Three were anaplastic meningiomas, two were papillary meningiomas, one was an atypical meningioma, and one was a sarcoma transformed from a meningioma with cervical lymph node metastasis. All patients had previously undergone repetitive surgeries and radiotherapy. Follow-up images were available for six patients with an observation period between 7 and 13 months. We applied ^{18}F-boronophenylalanine (BPA)-positron emission tomography (PET) before BNCT in six of the seven patients. One patient underwent methionine-PET instead of ^{18}F-BPA-PET.

RESULTS: Five of the six patients who underwent BPA-PET analysis showed good BPA uptake, with a greater than 2.7 tumor-to-healthy brain ratio. The atypical meningioma case showed a tumor-to-healthy brain ratio of 2.0. The original tumor sizes were between 13.6 and 109 ml. Two of the three anaplastic meningiomas showed a complete response, and all six patients available for follow-up imaging showed radiographic improvements. Clinical symptoms before BNCT, such as hemiparesis and facial pain, were improved after BNCT in all but one patient. In this patient, a huge atypical meningioma arose from the falcotentorial junction and extended to the bilateral occipital lobes and brainstem; visual problems worsened after repetitive BNCT, with an increase in peritumoral edema.

CONCLUSION: Malignant meningiomas seem to be good candidates for BNCT.

KEY WORDS: Boron neutron capture therapy, Boronophenylalanine positron emission tomography, Malignant meningioma, Sarcoma

Neurosurgery 61:82–91, 2007 DOI: 10.1227/01.NEU.0000255434.47044.41 www.neurosurgery-online.com

The management of malignant meningiomas (MM) remains a challenge. In a large series of atypical and anaplastic meningiomas, the recurrence rate of these tumors has been reported as 78 to 84% within 5 years (8, 19). The median survival of patients has been reported as 6.89 years, and the rate of late mortality caused by recurrence has been reported as 69% after the initial surgery (19). Although some treatments for recurrent MMs have been reported, a standard treatment has not yet been developed.

We propose a novel radiation modality for the treatment of MMs. Boron neutron capture therapy (BNCT) is a targeted radiation approach that significantly increases the therapeutic ratio relative to conventional radiotherapeutic modalities. BNCT is a binary approach: a ^{10}B-labeled compound delivers high concentrations of ^{10}B to the target tumor, relative to the surrounding healthy tissues. This is followed by irradiation with thermal or epithermal neutrons that become thermalized at a certain depth within the tissues. The short range (<10 μm) of the α and ^{7}Li particles released from the ^{10}B(n,α) ^{7}Li neutron capture reaction makes the microdistribution of ^{10}B critically important in therapy (24). These particles have high linear energy transfer. These characteristics contribute to the tumor-selective and strong tumoricidal activity of BNCT, combined with the negligible damage to healthy tissue.

TABLE 1. Parameters of boron neutron capture therapy for each patient[a]

Patient no. (tumor type)	BNCT	BSH[b]	BPA[c]	Tumor (Gy-Eq)		Brain (Gy-Eq)	Remarks
				Max	Min	Max	
1 (papillary)	1st	5 g	500 mg/kg/3 h	93.9	39.7	11.3	
	2nd (5 mo after)	5 g	700 mg/kg/3 h	73.2	44.2	13.1	
2 (anaplastic)[d]	1st	5 g	500 mg/kg/h	55.1	29.8	10.3	
	2nd (4 mo after)	—	700 mg/kg/3 h	81.6	22.9	14.6	Incomplete because of motion
	3rd (5 mo after)	—	700 mg/kg/3 h	55.9	22.3	9.32	
3 (anaplastic)		5 g	500 mg/kg/3 h	49	32	8.69	
4 (papillary)	1st	5 g	500 mg/kg/3 h	71.8	22.1	8.75	
	2nd (1 mo after)	—	700 mg/kg/4 h	81.6	22.9	14.6	
5 (sarcoma)	1st	2.5 g	700 mg/kg/4 h	48.3	7.62	7.92	30 min from right
				55	6.73	9.12	30 min from left
	2nd (2 wk after)	2.5 g	700 mg/kg/4 h	49.5	11.7	8.25	30 min from right
6 (atypical)	1st	2.5 g	700 mg/kg/4 h	65.2	19	11.8	
	2nd (3 wk after)	2.5 g	700 mg/kg/4 h	67.4	20.5	12	

[a] BNCT, boron neutron capture therapy; BSH, sodium borocaptate; BPA, boronophenylalanine; max, maximum; min, minimum.
[b] BSH, 5 g (1 h drip, 13 h before irradiation); 2.5 g (1 h drip, 1 h before irradiation).
[c] BPA, in 4 h drip, 3 h before irradiation and approximately 1 h during irradiation.
[d] Patient 2, 2nd and 3rd were applied for subcutaneous invasion of the tumor in temporal and infratemporal lesions.

Therefore, if sufficient quantities of boron compounds can be made to accumulate selectively in tumor tissues, BNCT could be an ideal radiotherapy.

In the past 4 years, we treated 41 patients who had malignant gliomas with BNCT (14) with two boron compounds, sodium borocaptate (BSH) and boronophenylalanine (BPA), for which the accumulation mechanisms differ (17). In this series, we used similar protocols for the BNCT, with some modifications for MMs compared with malignant gliomas. We previously reported the first case of a papillary meningioma (World Health Organization Grade 3) successfully treated by BNCT (Patient 1 in *Tables 1–3*) (23). Here, we introduce cumulative clinical results for BNCT for malignant tumors related to meningiomas, especially regarding radiographics. We also discuss the indications and limitations of this unique treatment for MMs.

PATIENTS AND METHODS

Patients

Seven patients with malignancy related to meningiomas were treated with BNCT between June 2005 and January 2006. Three malignancies were anaplastic meningiomas, two were papillary meningiomas, one was an atypical meningioma, and one was a sarcoma transformed from meningioma with cervical lymph node metastasis. The six patients listed in *Table 1* were followed-up with neuroimaging. One of the cases of anaplastic meningioma was excluded from follow-up because of an accidental femur fracture. All patients were referred to our institution for BNCT because of uncontrolled tumor growth after repetitive surgeries and fractionated external radiotherapy (XRT) or stereotactic radiosurgery (SRS).

^{18}F-boronophenylalanine-Positron Emission Tomography Analysis

The patients underwent ^{18}F-boronophenylalanine (BPA)-positron emission tomography (PET) analysis to assess the distribution of BPA and to estimate the boron concentrations in tumors before neutron irradiation. Here, BPA was one of the two boron compounds used for the treatment, as described above for our BNCT treatment for malignant glioma. The tumor-to-normal brain (T/N) ratio of BPA uptake was estimated from this PET study, and dose planning was performed according to the T/N ratio. *Figure 1* shows representative data from this PET study. The PET study was omitted in one case of an anaplastic meningioma (Patient 3) because of trouble with the machine. The patient was analyzed with ^{11}C-methionine PET instead of ^{18}F-BPA-PET.

Clinical Regimen of BNCT for MMs

This project was approved by the Ethical Committee of Osaka Medical College, Takatsuki City, Japan and the Kyoto University Committee for Radiation Therapeutics, Kyoto, Japan. In addition, each candidate was discussed and approved by the latter committee. The clinical regimen of BNCT for MMs was modified somewhat from that for malignant gliomas (14). Principally, the patients were administered BPA with or without BSH. BPA (99 atoms% ^{10}B, L-isomer) was supplied by the Stella Chemifa Corporation (Osaka, Japan). BSH (99 atoms% ^{10}B) was purchased from Katchem, Ltd. (Prague, Czech Republic). During the study period, BSH was difficult to obtain in the world market. Therefore, in some cases, BSH administration was impossible and omitted (in the second and third BNCT of Patient 2 and in the second BNCT of Patient 4; see *Table 1*), and, in some cases, we used half the amount of BSH (2.5 g/body) just 1 hour before the neutron irradiation (in Patients 5 and 6). Otherwise, 12 hours before the neutron irradiation, the patients were administered 5 g of BSH intravenously for 1 hour. This BSH administration was applied at Osaka Medical College.

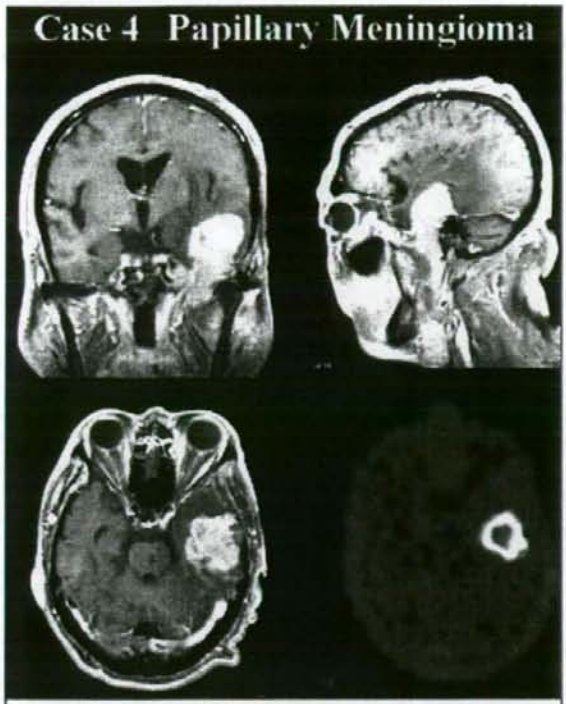

FIGURE 1. *Representative ^{18}F-BPA-PET and corresponding Gd-enhanced 3-D MRI scans from Patient 4. A homogeneously enhanced mass can be seen in each MRI scan. The tumor was in the left middle cranial fossa with perilesional cerebral edema and extended to the infratemporal fossa. ^{18}F-BPA-PET study revealed marked accumulation of BPA. The T/N ratio was calculated as 5.0.*

Early in the morning of the neutron irradiation, the patients were transferred from Osaka Medical College to Kyoto University Research Reactor Institute by ambulance and were administered 500 or 700 mg/kg of BPA intravenously for 3 hours before the irradiation. Principally, 700 mg/kg of BPA was used when BSH was not available for the treatment to increase the boron concentrations in the tumor tissue. In Patients 4, 5, and 6, BPA was administered at 200 mg/kg/h for 3 hours, and 100 mg/kg of BPA was kept to be administered during the irradiation (see *Table 1*). Blood was sampled every 30 minutes to 1 hour after boron compound administration until the neutron irradiation was completed, and the boron concentrations in the blood were monitored. The boron concentrations from BSH in the tumor and brain tissue were estimated in the same manner as the boron concentration from BSH in blood. The boron concentrations from BPA in the tumor and healthy brain were also estimated by the T/N ratio of ^{18}F-BPA on PET. Based on these boron concentrations contributed by each boron compound, the neutron fluence rate simulated by the dose-planning system Simulation Environments for Radiotherapy Applications (Idaho National Engineering and Environmental Laboratory, Idaho Falls, ID), and the previously reported factors related to the relative biological efficacy of neutron beams, BPA, and BSH (2, 15), the total dose to tumor and healthy brain could be estimated. The patients were positioned in front of the collimator at Kyoto University Research Reactor Institute. The neutron irradiation time was determined not to exceed 15 Gy-Eq to the healthy brain. Here, Gy-Eq means a biologically equivalent x-ray dose that can give equivalent effects in total BNCT radiations. Epithermal neutron irradiation was performed without craniotomy and without anesthesia. After treatment, the doses administered were precisely re-estimated.

Assessment of Effectiveness

The effectiveness of this treatment was volumetrically assessed in serial radiographic analysis. Magnetic resonance imaging (MRI) scans were performed with a slice thickness of 7.5 mm. The images were analyzed using a software package (Scion Image, v. Beta 4.0.2; Scion Corp., Frederick, MD). The contrast-enhanced area was measured in each slice and recorded in square millimeters. The values for the area were then multiplied by the thickness of the slice (7.5 mm) to obtain the volume. Follow-up images were obtained every 1 or 2 months.

RESULTS

Parameters of BNCT in Each Patient

The parameters of BNCT for each patient are listed in *Tables 1* and 2. The tumor sizes before BNCT varied from 13.6 to 109 ml. Five of the six patients underwent a BPA-PET study. In this series, the T/N ratios of ^{18}F-BPA determined by the PET study were 2.0 to 5.0. The mean value of the T/N ratio in this series is 3.7, which includes the T/N ratio of the patient for whom follow-up imaging could not be obtained. In our malignant glioma series, the T/N ratio of the 16 cases of recurrent glioblastoma was 3.8 (unpublished data). This value is almost the same as that for the current meningioma series.

In principle, we did not intend to use a neutron irradiation time of longer than 1 hour per treatment. We also determined the putative curative dose for the tumor to be 40 Gy-Eq. Therefore, in cases in which the Simulation Environments for Radiotherapy Applications simulation indicated that we would not obtain a minimum tumor dose of more than 40 Gy-Eq within 1 hour of neutron irradiation, we intentionally adopted fractionated BNCT with a 1 to 4-week interval.

ILLUSTRATIVE CASES

Patient 2

Patient 2 was a 48-year-old woman who had undergone five surgeries during the preceding 2 years, with a histological diagnosis of anaplastic meningioma and had received 60 Gy XRT (40 Gy for the whole brain and 20 Gy locally) and one SRS (18 Gy as the marginal dose). No residual tumor was observed after the first four of these surgeries. After the last surgery, however, a part of the tumor was found to have infiltrated the right sigmoid sinus. She was referred to our clinic because of uncontrollable lesions in the right parietal and occipital regions with meningitis. After admission to our institute, her scalp was opened by an epidural abscess. She was drowsy and in a bedridden stage at the time of admission. After primary closure of her operative wound, we performed BNCT. MRI scanning just before the first BNCT revealed two enhanced lesions in the right parietal and occipital regions and an equivocal lesion in the temporal lobe. No apparent mass was identified on the surface of the right cerebellum on this MRI scan. BPA-PET, however, revealed uptake of BPA at the parietal, occip-

TABLE 2. **Radiographic improvement of the patients by boron neutron capture therapy**[a]

Patient no. (tumor type)	Initial volume (ml)	T/N ratio	Measurement 1 (%) (time of measurement)[b]	Measurement 2 (%) (time of measurement)[c]	Follow-up duration (mo)[d]	TTP (mo)
1 (papillary)	65.6	5	74.6 (0.5 mo)	38.7 (4 mo)	13	NR
2 (anaplastic)	13.6	2.8	0 (4 mo)		12	NR
	194.0		24.7 (2 mo from 2nd) (subcutaneous plus temporal plus cerebellum)	19.2 (4 mo from 2nd)		NR
3 (anaplastic)	25.7[f]	ND	33.9 (5 wk)	0 (4 mo)	12	NR
	4.9[g]		122.0 (5 wk)	48.3 (4 mo)		6 mo
4 (papillary)	69.5	5	57.5 (1 mo)	30.2 (4 mo)	9	NR
5 (sarcoma)	109[h]	2.7	45.9 (6 wk)	35.0 (5 mo)	7	NR
	17.4[i]	3	4.3 (6 wk)	0 (5 mo)		NR
6 (atypical)	92.7	2	76.3 (6 wk)	70.3 (7 mo)	7	NR

[a] T/N, tumor-to-normal ratio; TTP, time to progression; NR, no recurrence; ND, not determined.
[b] Neuroimaging taken within 2 months after BNCT.
[c] Neuroimaging that showed the best response by BNCT.
[d] Duration between BNCT and the end of July 2006 (time of manuscript submission).
[e] See Addendum.
[f] Main tumor mass.
[g] Concomitant lesion close to superior sagittal sinus.
[h] Main tumor mass.
[i] Lymph node metastasis.

ital, and temporal lesions, and at the surface of the right cerebellum. We applied the first BNCT to the apparent tumors in the right parietal and occipital regions and observed the temporal and cerebellar lesions because of the possibility of inflammation. After the first BNCT, the original lesions of the parietal and occipital lobes continued to shrink during the observation period, and no apparent enhancement was recognized in these regions, as shown in *Figure 2*. The skin defect was covered with a vascularized musculocutaneous flap after the first BNCT. After the operation, she was discharged from our hospital in a wheelchair and her mental state was almost alert. One month after the skin repair, large subcutaneous, temporal, and cerebellar masses were recognized on MRI scans (total volume, 192 ml; see *Fig. 2*; *Table 2*). She was bedridden again because of cerebellar signs. She was treated with a second and third BNCT at 4 months after the first BNCT. The temporal and cerebellar lesions disappeared completely after these BNCTs, and the subcutaneous lesion also shrank markedly. The tumor size became less than 20% in this lesion 4 months after the repetitive BNCTs, whereas a high intensity was observed in the right temporoparietal lesion on a T2-weighted MRI scan 8 months after the first BNCT. At the time of the preparation of this manuscript, the patient was in a terminal state; however, despite metastasis of the meningioma to the cervical lymph nodes and thoracic paravertebral and right parakidney areas, and a huge mass in the pelvic area, as demonstrated by a systemic BPA-PET study (data not shown), she can still enjoy conversation with her family.

Patient 3

Patient 3 was a 60-year-old woman who had undergone five surgeries and one SRS (20 Gy as the marginal dose) with a histological diagnosis of anaplastic meningioma during the 18 months before her referral to our clinic. She had experienced right hemiparesis after her last surgery, which worsened slightly while waiting for BNCT. Two gadolinium (Gd)-enhanced lesions were identified on the MRI scan just before BNCT. The main tumor mass was in the left frontoparietal convexity with subcutaneous extension, and the other small mass was close to the superior sagittal sinus (SSS). She could not receive ^{18}F-BPA-PET because of trouble with the machine. Therefore, we used a T/N ratio of 3.0, obtained from ^{11}C-methioinine PET instead of ^{18}F-BPA-PET. ^{11}C-methioinine accumulation was recognized only in the main tumor and not in the small mass close to the SSS. At the BNCT, the collimator was centered between the two masses so that both could be treated simultaneously. Four months after BNCT, no contrast enhancement was recognized on the follow-up image where the main tumor had been, the concomitant small mass close to the SSS was reduced in size (*Fig. 3*), and the hemiparesis was slightly improved by rehabilitation. However, 6 months after BNCT, the patient's right hemiparesis became aggravated, with a slight increase in brain edema. We began administration of a small amount of steroids to control this edema. Follow-up MRI scans obtained 6 and 9 months after BNCT revealed the occurrence of an enhanced lesion between the original main tumor and the lesion close to the SSS, and the latter lesion itself was enlarged. On follow-up ^{18}F-BPA-PETs, uptake of tracers became apparent in the mass close to the SSS, whereas faint uptake of the tracers was identified in the new lesion. We removed the mass close to the SSS via another craniotomy and confirmed tumor tissue with some degeneration of this lesion, whereas only radiation necrosis was identified in the newly appeared lesion on MRI scanning.

Patient 4

Patient 4 was a 67-year-old man who had undergone surgery 2 years earlier with a histological diagnosis of papillary meningioma; he had undergone another operation and received radiation of 54 Gy XRT during the 2 years before admission to our clinic. He also experienced a brainstem cerebral infarction during this period. Regardless of these treatments, his mass grew rapidly without any effects from the XRT. *Figure 1* shows the Gd-enhanced MRI scan on admission and the BPA-PET scan. The tumor was in the middle cranial fossa with infratemporal extension. BPA-PET study revealed a marked accumulation of BPA. The T/N ratio was calculated as 5.0. He received BNCT two times, with an intentional interval of 1 month. His head above the enhanced lesion was protected with a lithium plate to decrease the absorbed dose in his healthy brain. The tumor shrunk rapidly with repetitive BNCTs (*Fig. 4*).